Energy Reports 11 (2024) 4784–4811

Contents lists available at ScienceDirect

Energy Reports

journal homepage: www.elsevier.com/locate/egyr

Research paper

Investigation of the integration of an oscillating aerofoil-based energy harvester into the building roof

Katrina Calautit *, Cameron Johnstone

Department of Mechanical and Aerospace Engineering, University of Strathclyde, Glasgow, UK

ARTICLE INFO

Keywords:
Computational fluid dynamics (CFD)
Numerical modelling
One degree of freedom
Wind energy
Oscillating aerofoil
Building energy

ABSTRACT

The increasing energy efficiency requirements have led to innovative renewable energy solutions being integrated into buildings. Several works have shown the potential of micro wind turbines on buildings. However, their implementations have been hindered by several challenges. Flow energy harvesting devices such as oscillating aerofoils provide potential, yet a literature gap exists regarding their integration into buildings. This study addresses this gap by investigating oscillating aerofoil wind energy harvesting system performance through numerical modelling. A coupled numerical model was introduced, integrating a novel computational approach using ANSYS Fluent with one degree of freedom in rotational motion. This methodology was introduced to analyze the dynamic behaviour and predict mechanical power output of the oscillating aerofoil wind energy harvesting system, which is a novel exploration in existing literature. Moreover, validation of the computational fluid dynamics model was conducted through using experimental wind tunnel data in the literature, and results demonstrated agreement between numerical and experimental results. To improve the wind energy harvesting system of a single oscillating aerofoil, it was integrated into building roof to take advantage of acceleration effects of building roof shape. The design improvement comprises of a novel wind energy harvesting system design of an oscillating aerofoil integrated into three different building roof including flat, pitched, and curved shapes to enhance energy efficiency. The numerical analysis demonstrated that integrating an oscillating NACA 0012 aerofoil into a curved roof resulted in the highest average power output. Specifically, the integration of the curved roof and the aerofoil yielded 18 watts, while the flat roof generated only 0.6 watts at a wind speed of 3 m/s. Integration into a pitched roof achieved 12 watts at 9 m/s. Comparatively, integrating the curved roof with the aerofoil increased power output by 50% compared to the pitched roof design at 9 m/s wind speed. Thus, variations in wind speed significantly impact performance. In addition, changes in wind direction from 0 to 10 degrees led to reduced efficiency and lower predicted power output. Lastly, the power spectral density for NACA 0012 integrated into the pitched and curved roof buildings revealed peaks at 5.8 Hz in 9 m/s wind speed conditions.

1. Introduction

In recent years, there has been growing interest in the installation of building-integrated wind energy harvesting technology (Østergaard et al., 2021). Wind energy capture systems have long been recognized as a prominent strategy for integrating sustainable energy into the built environment, with their popularity spanning several decades (Xu et al., 2021a). Extensive studies have been conducted on integrating traditional micro or small-scale wind energy harvesting technologies into buildings. This includes the utilization of vertical axis wind turbines (VAWT), horizontal axis wind turbines (HAWT), and ducted wind turbines (DWT). Research of (Xu et al., 2021a) has indicated that these technologies can take advantage of wind speed acceleration surrounding building structures (Ntinas and Zhang, 2014; Lu and Ip, 2009; Ledo and Kosasih, 2011), thus increasing the amount of power harvested from airflow. However, despite their potential benefits, conventional wind turbines experience obstacles (Cao et al., 2022) when installed and

Abbreviations: BI-WEHS, Building-Integrated Wind Energy Harvesting System; AOA, Angle of attack; 2D, Two-dimensional; 3D, Three-dimensional; URANS, Unsteady Reynolds-averaged Navier-Stokes; SIMPLE, Semi-Implicit Method for Pressure-Linked Equations; ABL, Atmospheric Boundary Layer; ROMs, Reduced Order Models; CFD, Computational Fluid Dynamics; DOF, Degree of Freedom; DWT, Ducted Wind Turbine; HAWT, Horizontal Axis Wind Turbine; VAWT, Vertical Axis Wind Turbine; VIV, Vortex-Induced Vibration; AIJ, Architectural Institute of Japan; PSD, Power Spectral Density; FFM, Fast Fourier Transform.

* Corresponding author.
E-mail address: katrina.calautit@strath.ac.uk (K. Calautit).

https://doi.org/10.1016/j.egyr.2024.04.022
Received 17 November 2023; Received in revised form 23 March 2024; Accepted 14 April 2024

Nomenclature

Symbols

U (m/s)	Air velocity
P (Pa)	Pascal
g (m/s2)	Gravitational acceleration
τ (N.m)	Torque
ω (rad/s)	Angular velocity
t (s)	Time
(n-m/rad)	Newton metre per radian
L (m/mm)	Length
F (N)	Force
(x, y, z)	Direction
f (Hz)	Frequency
P (watts)	Power
$\Delta\theta$	Angular rotation
Δt	Rate of change of angular velocity
W (kg)	Weight

operated within buildings, including high costs, reduced wind speeds, turbulence in urban settings (Xu et al., 2021b), vibrations, and placement challenges (Aravindhan et al., 2022).

1.1. Research gaps and novelty

To address these obstacles, this study presents an innovative method for harnessing energy from wind flow around buildings. The proposed approach comprises of wind energy harvesting device utilizing an oscillating aerofoil. Notably, despite existing research (Bhat and Govardhan, 2013) on the technical performance of stand-alone (Poirel and Harris, 2008) or isolated oscillating aerofoil devices (Tang and Dowell, 2016; Hamlehdar et al., 2019), none have explored the integration of these systems into building structures, such as roofs (Chong et al., 2013; Wang et al., 2018). In addition, the impact of the building structure on the oscillating aerofoil system for power generation and energy harvesting efficiency remains unexplored (Li et al., 2018; Naseer et al., 2017; Chai et al., 2021a). Moreover, the influence of the external wind environment (Aquino et al., 2017a; Quy et al., 2016) on these energy harvesters has received limited attention. Research on the effect of atmospheric boundary layer (ABL) profile and terrain on the efficiency of such energy capture systems is scarce (Naseer et al., 2017). Lastly, experimental investigations on small or micro energy harvesting technologies integrated into buildings are limited (Quy et al., 2016). This study aims to address these gaps by investigating the feasibility and effectiveness of integrating oscillating aerofoil-based wind energy harvesting systems into building structure.

In the assessment of air circulation around structures and the performance of energy harvesting technologies, computational fluid dynamics (CFD) modelling is widely employed and validated by the research community. It allows the prediction and analysis of wind flow patterns above and around buildings (Calautit and Hughes, 2014) and the aerodynamic characteristics of wind energy harvesters (Zhang et al., 2020). CFD serves as a cost-effective alternative to wind tunnel testing, enabling the exploration of various parameters across different wind and operational conditions (Fu et al., 2020). Specifically, there is a lack of exploration in the literature regarding the modelling and simulation of an oscillating aerofoil energy harvester integrated into building structures.

While many studies have utilized CFD to assess the performance of traditional wind turbines, there is a gap in the literature regarding the application of CFD to the specific scenario of an oscillating aerofoil integrated into building roof. For instance, research conducted by (Sanderasagran et al., 2020) employed Computational Fluid Dynamics (CFD) with the dynamic mesh method to examine power extraction and offshore wind turbine dynamics but did not focus on the integration of such systems into building structures. Similarly, the degree of freedom (DOF) solver method was utilized in (Dunbar et al., 2015) to investigate wind turbine behaviour in offshore environments, yet this method has not been extensively applied to the study of oscillating aerofoils integrated into building structures. In addition, the literature review reveals a lack of exploration utilizing the one degree of freedom (1 DOF) solver method for the analysis of oscillating aerofoils integrated into building roofs. Although this method has been predominantly used for offshore wind turbines undergoing pitch motion (Wicaksono et al., 2021; Tran et al., 2014; Cheng et al., 2019; Wang et al., 2022), its application to the specific design, modelling, and setup conditions of oscillating aerofoils integrated into building structures remains unexplored. Hence, further research in this field is vital to enhance the comprehension of the dynamics and efficiency of oscillating aerofoil energy harvesters when integrated into building structures.

1.2. Aims and objectives

This study aims to predict and analyse the aerodynamic characteristics, dynamics of pitch oscillation, and power extraction efficiency of a wind energy harvester using an oscillating aerofoil with the NACA 0012 profile integrated into a building roof. In this study, it is referred to as a Building Integrated Wind Energy Harvesting System (BI-WEHS). A model representing the introduced design of oscillating aerofoil with the NACA 0012 profile integrated into a building roof will be modelled and simulated in three-dimensional (3D) using the Unsteady Reynolds-Averaged Navier-Stokes (URANS) approach in ANSYS Fluent. The simulation will utilise the STANDARD k-epsilon turbulence model and a solver with one degree of freedom (1 DOF). The standard k-epsilon turbulence model is widely employed in CFD analyses due to its computational efficiency, robustness, and extensive validation. It strikes a balance between accuracy and computational resources, making it suitable for various engineering applications. However, for complex flow phenomena, more advanced turbulence models may be necessary. The SIMPLE (Semi-Implicit Method for Pressure-Linked Equations) algorithm was employed to solve the Navier-Stokes equations in computational fluid dynamics (CFD). The process includes estimating the pressure distribution and solving the equations of motion to derive velocity components and introducing a corrective pressure to maintain continuity.

When integrating rotational motion through dynamic mesh in software platforms such as ANSYS Fluent, modifications were made to the mesh to account for and adapt to the changing geometry caused by the rotational motion. The governing fluid flow equations remain the same, while additional equations are introduced to describe mesh deformation and updates. Accurate simulation of fluid flow around moving or rotating geometries requires defining proper boundary conditions and mesh interfaces. In the context of vortex-induced vibrations (VIV) simulations, the dynamic mesh method and one degree of freedom (1 DOF) rotational motion were applied to study the interaction between fluid and solid in an oscillating aerofoil with the NACA 0012 profile integrated into the building. Through accurately capturing the dynamic motion and displacement of the aerofoil, these simulations provided insights into the aerodynamic behaviour of the system.

Fig. 1 depicts the schematic and computational model of the introduced design presenting an oscillating NACA 0012 aerofoil integrated into a building roof for wind energy capture. The energy conversion process from wind kinetic energy to electrical energy using oscillating aerofoils. Wind flow imparts kinetic energy to the aerofoil, inducing oscillations, representing the conversion of wind kinetic energy into mechanical energy. This mechanical energy is then transferred through a system consisting of a motor and generator. The motor converts it into rotational motion, and the generator further transforms this into electrical energy through electromagnetic induction, serving as the final

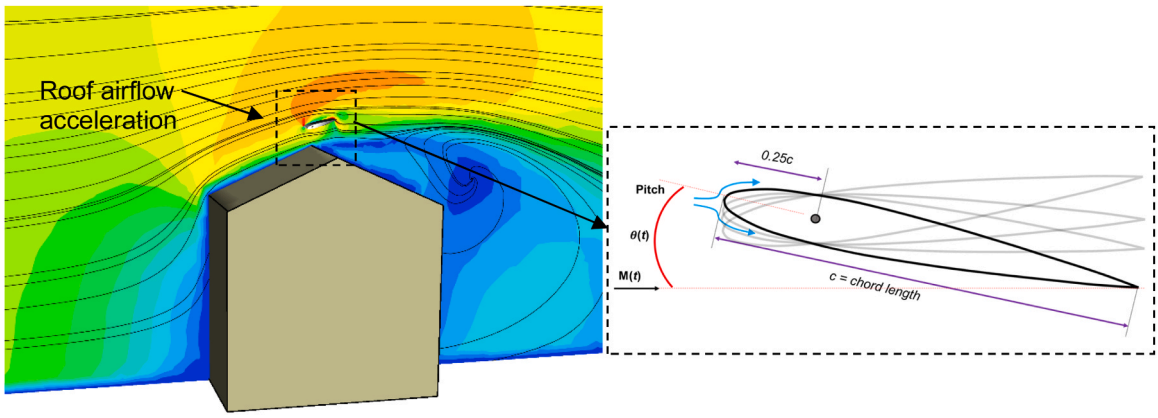

Fig. 1. Schematic diagram of the integration of the oscillating NACA 0012 aerofoil into the building roof structure.

usable electrical output. In this configuration, airflow starts the oscillating motion of the NACA 0012 aerofoil, driven by wind-induced torque on the supporting rod, with contributions from the inertia and weight of the aerofoil. The configuration of the roof influences airflow velocities and turbulence intensity, impacting the potential power output of the proposed system, particularly at higher wind speeds (Abohela et al., 2012)

The following sections of this paper are structured as follows: Section 2 addresses the identified research gap through a comprehensive literature review. While in Section 3, it outlines the research methodology, focusing on the utilization of ANSYS Fluent to model the one-degree-of-freedom (DOF) rotational motion. This approach allows for an in-depth investigation into the dynamic behaviour and fluid-solid interaction of the integrated design comprising an oscillating aerofoil and building roof. Section 4 examines the results and discussions, providing insights gathered from the analysis. Lastly, Section 5 presents the conclusions drawn from the study and offers recommendations based on the findings.

2. Literature review

This section presents a summary of the latest developments in systems for harvesting wind energy integrated into buildings. The conventional types of BI-WEHS include the HAWT, VAWT, and DWT, which have been studied for the past few decades and proved to provide useful power output in watts to kilowatts. Nevertheless, the deployment of these wind energy harvesting systems in rural or urban buildings has certain challenges and limitations. These include the power output, high cost, weight of the wind turbine, vibration, and noise pollution issues. Due to these challenges, researchers and engineers continue to find the best wind energy harvesting systems that are suitable for different environments and wind speeds.

Recently, there has been significant growth in the topic area of miniature wind energy harvester systems, as evidenced by numerous studies and research articles (Akaydin et al., 2012; Abdelkefi and Hajj, 2012; Bryant et al., 2012a; Hobeck, 2014; Bibo, 2014; Zhao, 2015; McCarthy et al., 2016). These studies have focused on utilising aeroelastic instabilities such as aeroelastic flutter (Bryant et al., 2012b), and vortex-induced oscillation or vibration to harness wind power more effectively (Akaydin et al., 2012). Scholars have conducted research on utilising aeroelastic instabilities, including aeroelastic (Bryant et al., 2012b) vortex-induced vibration (VIV) (Akaydin et al., 2012), and galloping mechanism (Zhao and Yang, 2015) for harnessing wind power. Researchers have reported their findings in various publications, providing insights into the potential of these technologies for capturing wind energy at a small-scale. Deploying wind energy capture technologies based on wind-induced vibrations on commercial building structures offers several benefits, including bringing power generation closer to users (Calautit and Johnstone, 2023) This can lead to a more efficient distribution of power to consumers, increased energy efficiency, reduced carbon footprint, and decreased reliance on the grid.

In addition, a decentralised power grid system can reduce the costs associated with transmitting power over long distances and decrease the dependence on diesel generators for electricity generation. Through generating power locally, the need for costly transmission infrastructure is reduced, and communities can become less dependent on fossil fuel-based generators (Calautit and Johnstone, 2023). Moreover, this system can be a feasible solution for delivering renewable and sustainable energy in small-scale settings and for powering self-charging technologies with a simple and compact design. With generating power locally, it can directly provide electricity to building occupants, making it an efficient and effective solution for micro-energy needs. The proposed model of BI-WEHS can also directly power wireless sensor networks, monitoring devices, LED lights, and small-scale electronic devices within buildings. These features are appropriate for wind energy capture systems in regions with low wind speeds and lower costs for installation and operation in comparison to existing commercialised wind turbines (Calautit and Johnstone, 2023).

ANSYS CFD software has been a useful tool to simulate the airflow patterns over and around buildings. This facilitates the examination of optimal designs and placement of wind energy harvesting systems both above and around buildings to optimise performance. As computing capacity has increased, CFD modelling has become a crucial tool for numerical analysis, particularly regarding wind conditions and various environmental settings. Recent advancements in wind energy harvesting systems using CFD simulations demonstrated developments from wind flow modelling around aerofoil to atmospheric boundary layer (ABL) through arrangements of wind farms or turbines (Calautit et al., 2018).

Ayhan and Sağlam (2012). examined three distinct CFD model scenarios of wind turbines, encompassing vertical axial Darrieus and Savonius turbines, and horizontal axial propeller integrated within urban and rural residential environments. The study affirmed its capability to assess the efficiency of wind energy harvesting technologies in areas with optimal wind energy resources while avoiding turbulent zones. Studies of (Aquino et al., 2017a, 2017b; Walker, 2011; Reja et al., 2022) were also focused on the wind resources assessments using CFD simulations and were of great interest to many researchers and engineers to predict and evaluate the airflow distribution around and above the building roof structures. Another study, conducted by Toja-Silva et al (Toja-Silva et al., 2018). involved CFD simulations to examine the airflow around a building. The objective was to qualitatively evaluate the impact of a dynamically fluctuating airflow environment on wind turbines integrated into the building roof.

The use of high-fidelity CFD method in combination with one degree of freedom simulations has certain benefits over using other engineering models. 1 DOF simulations can provide a more accurate solution by only

requiring the geometry and mass specifications of the CFD model, although the method is computationally more expensive (Patel and Henderson, 2003) The dynamic mesh method allows for modelling fluid flows in situations where the computational domain shape undergoes changes over time due to movement along the domain boundaries. Through integrating a 1 DOF solver, this method can accurately determine the trajectory of a moving object, based on the aerodynamic forces present in the surrounding flow field (Zhu et al., 2020). Several studies on 1 DOF and CFD solvers have been developed for simulating offshore oil platform dynamics, as referenced in studies (Tan et al., 2013; Xu et al., 2022; Kim et al., 2011; ANSYS, 2009). However, it is worth noting that these solvers use proprietary or closed-source software to calculate the 1–6-DOF equations of motion and Navier–Stokes equations in a coupled approach (Tan et al., 2013; Xu et al., 2022; Kim et al., 2011; ANSYS, 2009).

Based on the review of relevant research findings, it can be implied that the suggested model of integrating an oscillating aerofoil into the structure of a building roof has not been explored. Moreover, the CFD combined with one to six degrees of freedom simulations are usually used for offshore wind turbine simulations (Tan et al., 2013; Xu et al., 2022; Kim et al., 2011; ANSYS, 2009). The literature lacks exploration of the interaction between fluid (wind flow) and solid (wind energy harvester integrated into the building roof structure), especially regarding the utilisation of dynamic mesh and DOF methods.

3. Methodology

This section introduces the numerical, verification, and validation methods applied to evaluate the performance of an oscillating aerofoil integrated into the building roof structure. The numerical modelling section intoroduces the theory, 3D modelling of the geometry and domain, mesh generation and verification, mesh and time steps sensitivity analyses, setting up bundary conditions, and validation of CFD results against experimental data.

To model the 1 DOF rotational motion, specifically the pitch oscillation, of an object with a dynamic mesh in the y-axis direction, The equation of motion can be deduced by applying Newton's second law, and it can be expressed in Eqs. (1) and (2) (ANSYS, 2009).

$$I \bullet \frac{d^2\theta}{dt^2} + c \bullet \frac{d\theta}{dt} k \bullet \theta = M(t) \tag{1}$$

$$0.4 \bullet \frac{d^2\theta}{dt^2} + 850 \bullet \frac{d\theta}{dt} + k \bullet \theta = M(t) \tag{2}$$

where: θ represents the angular displacement of the object (pitch angle) in radians.

t represents time in seconds. I represent the object's moment of inertia around the pitch axis, measured in kg·m^2. c stands for the damping coefficient, measured in N·m·s/rad. k is the stiffness coefficient in N·m/rad. M(t) is the external moment acting on the object due to aerodynamic forces or other applied loads in N·m.

The stiffness coefficient (k) was not provided. The stiffness coefficient depends on the specific system and is typically determined by the structural properties of the object.

This equation represents the dynamic behaviour of the object undergoing pitch oscillation in the y-axis direction. The external moment, M(t), will depend on the specific conditions, forces, or loads acting on the object. To simulate this system using a dynamic mesh in ANSYS Fluent DOF solver with a 1 DOF constraint, additional equations and modifications would be required within the software to enforce the constraint and incorporate the dynamic mesh capability. Further discussions and equations may be required to analyze the impact of parameters such as the aerofoil stiffness coefficient (k) on system behaviour, particularly in scenarios involving different types of motion such as heave motion. The stiffness coefficient directly influences how the aerofoil responds to external forces, affecting its deformation and dynamic response. Higher stiffness results in less deformation and a more rigid response, while lower stiffness allows for greater flexibility and deformation. Dynamic mesh considerations become crucial in such cases, enabling adaptation of the computational mesh to accommodate the changing geometry of the aerofoil as it deforms during motion. This ensures accurate representation of the flow field and pressure distribution around the aerofoil throughout its motion.

In addition, sensitivity analyses were conducted to ensure the most suitable spring constant values for the proposed system, focusing on an oscillating aerofoil integrated into a building roof structure. These analyses showed that a spring constant of constant 850 (n-m/rad) was the most effective for our specific application. This choice was predicated on the observation that pitch oscillations maintained a continuous and stable pattern under this spring constant. Therefore, the values of constant 850 (n-m/rad), was most suitable under 3 m/s wind speed, 650 Nm/rad under 6 m/s, and 450 Nm/rad for 9 m/s. These values were selected as it ensured the desired stability and continuity in the oscillatory behaviour of the aerofoil, which is critical for the reliability and accuracy of our simulation results.

3.1. CFD geometry and domain

Fig. 2 depicts the CFD geometry, including a computational domain containing both the aerofoil and the building structure. The NACA 0012 aerofoil was selected for this investigation due to its widespread use in previous research on oscillating aerofoils for energy extraction. Furthermore, its well-known aerodynamic characteristics, supported by numerous published research data in the literature, which makes it a suitable choice. Table 1 provides specifications for the symmetrical NACA 0012 PVC foam aerofoil. Fig. 2(a) illustrates the symmetrical aerofoil with a rod mounted at 0.25 m chord length. The aerofoil size chosen is 1 m span and 1 m chord length, aligned with dimensions from prior research (Steenwijk and Druetta, 2023; Shuang et al., 2020; Rostamzadeh et al., 2012).

The decision to choose a different centre of rotation for the proposed design, specifically at 0.25c, is informed by various factors. This selection considers the aerofoil longer span and chord length, greater mass, and moment of inertia. Moreover, the integration of the aerofoil into the building roof structure implies an interaction with different wind behaviours. Previous studies, including those by (Fangwei and Sarkar, 2018; Xu and Yin, 2023; Zhu et al., 2023a, 2023b; Cao et al., 2023), provide insights into how factors such as roof structure design, building integration, mass distribution, and wind behaviour affect aerodynamic performance and aeroelastic behaviour.

The rod acts as a support for oscillatory motion, has a length of 0.015 m. This design choice is based on previous work by (Poirel and Harris, 2008) and aligns with theoretical principles and practical considerations. Placing the rod at the quarter-chord length optimizes aerodynamic balance, enhances energy harvesting efficiency, minimizes structural stresses induced by aerodynamic forces, and improves device durability and integrity. This approach also enhances stability and controllability, ensuring smoother and more predictable motion for effective energy harvesting. Previous studies and simulations provide empirical evidence supporting the favourable aerodynamic performance considerations of this approach (Poirel and Harris, 2008), Jamil et al., 2020 (Jamil et al., 2020). While the centre of gravity of the aerofoil is located at 0.42 m along the chord length, measured from the leading edge towards the centre of gravity of the aerofoil.

In Fig. 2(b), it shows the computational domain with a building measuring 6 m x 6.6 m x 6 m.

In this study, the selection of the computational domain size was guided by the Architectural Institute of Japan (AIJ) guidelines for practical applications of CFD to pedestrian wind environments around buildings. According to these guidelines: The lateral and top boundaries of the domain were set to be at least 5 times the height (5 H) of the target building. This distance is critical to minimize boundary effects on the

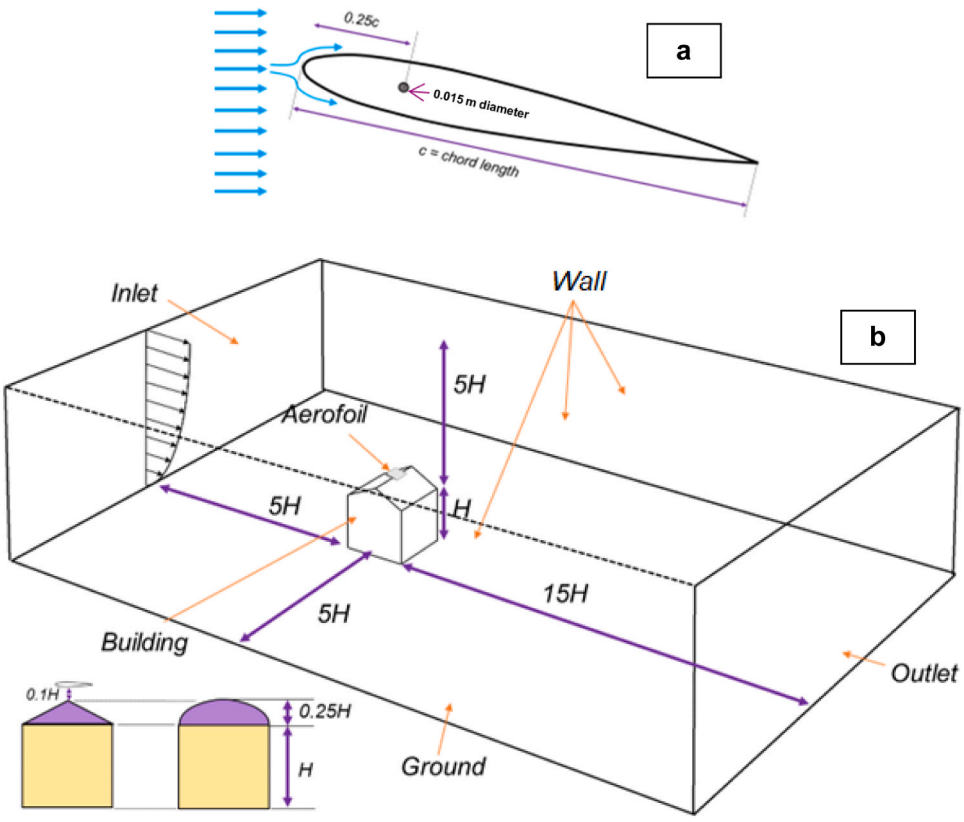

Fig. 2. (a) Aerofoil centre of rotation and rod diameter (b) schematic of the computational building and domain.

Table 1
Parameters of the oscillating NACA 0012 aerofoil applied in the CFD simulations.

Aerofoil profile	Dimension (m)	Mass (kg)	Moment of inertia (kg-m2)	Centre of rotation (m)	Centre of gravity location (m)
Symmetrical NACA 0012	1 meter span and 1 meter chord length	3.2	0.4	X - 0.25 Y – 0 Z - 0	X - 0.4182 Y - 0 Z - 0

airflow and to replicate an open environment. The inlet boundary was positioned to correspond to the upwind area covered by a smooth floor in wind tunnel tests, effectively replicating the approach flow conditions. The outflow boundary was placed at least 10 H behind the building, ensuring that the wake region was adequately captured and did not influence the inflow conditions. Through adhering to these guidelines, the aim was to ensure that the computational domain adequately represents the real-world conditions while minimizing the impact of boundary conditions on the flow field around the building. This approach is essential for accurately capturing the pedestrian-level wind environment in the vicinity of the building. Also, a detailed description of the domain size selection process, explicitly mentioning the adherence to the AIJ guidelines and the rationale behind each boundary placement relative to the building.

3.2. Mesh and verification

Fig. 3 shows the grid for the 3D CFD model created using ANSYS Meshing. The number of elements and nodes are shown in Table 2. The complexity of the model required the use of tetrahedral elements. The mesh analysis examined skewness, orthogonality, and aspect ratio criteria to ensure an appropriate mesh was generated. The maximum skewness value obtained was 0.7, which is within the acceptable range for highly skewed faces and cells. The minimum orthogonality quality achieved was 0.5 and the minimum aspect ratio mesh quality was 1.16.

It is noted that the importance of mesh quality in ensuring accurate CFD simulations. Given the values obtained for skewness, orthogonality, and aspect ratio, the mesh was refined to improve the accuracy of the results. Through refining the mesh, the integrity of the simulations and achieve more reliable predictions of fluid flow behaviour can be improved. In addition, the study indicates a thorough understanding of the mesh quality metrics and their significance in CFD simulations. The specific values for skewness, orthogonality, and aspect ratio were provided to demonstrate a comprehensive assessment of the mesh quality.

In summary, the selected mesh quality criteria and simulation setup appear well-suited for studying the fluid dynamics around an oscillating aerofoil integrated into a building roof structure. By ensuring appropriate mesh quality and utilizing a suitable turbulence model under transient conditions, the simulations can provide valuable insights into the aerodynamic behaviour and structural interactions, facilitating informed design decisions.

3.2.1. Mesh generation for BI-WEHS model

A sensitivity analysis of the computational grid was implemented by carrying out supplementary simulations with identical computational domains and boundary conditions but varying grid sizes. Grid refinement was conducted in alignment with critical zones of interest within the simulation of the integrated design involving an aerofoil and building roof structure. The mesh size was systematically adjusted to precisely capture regions with high gradients, as depicted in Fig. 3. This iterative process led to an augmentation in the number of elements, transitioning from coarse to fine resolution. The maximum error was observed at ±0.08 m/s and an average error of 1%. This was between the medium and fine mesh. Therefore, a reiteration of the CFD model with a fine mesh did not result in a significant change in the results.

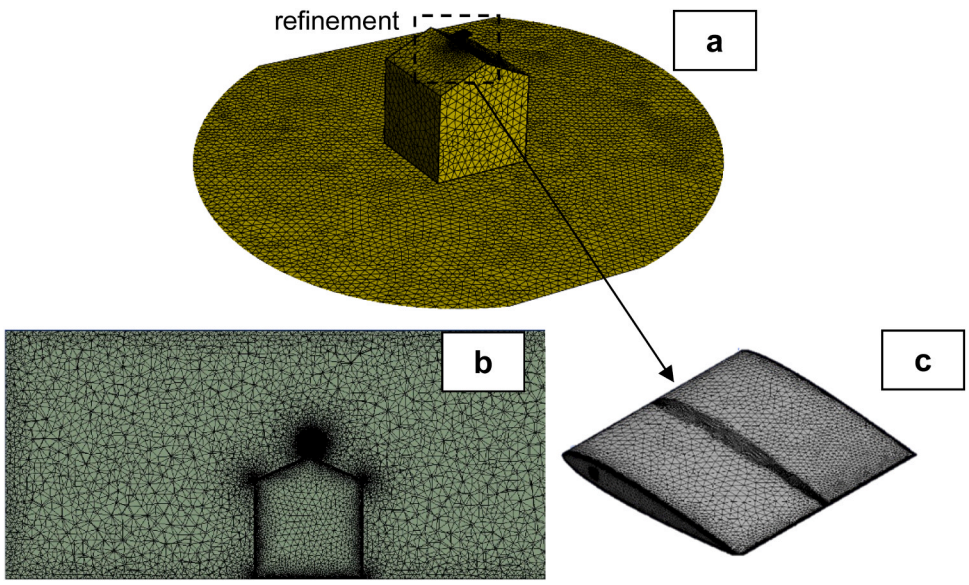

Fig. 3. (a) Mesh of the computational domain of the building with the oscillating NACA 0012 aerofoil integrated into the pitched roof (b) 2D view of the mesh for BI-WEHS model (c) Surface mesh around the oscillating aerofoil.

Table 2
Mesh size details for three parameters.

NACA 0012 integrated into the flat roof building			NACA 0012 integrated into the pitched roof building			NACA 0012 integrated into the curved roof building		
Mesh	Nodes	Elements	Mesh	Nodes	Elements	Mesh	Nodes	Elements
Fine	368587	1996799	Fine	369663	2002791	Fine	375320	2033751
Medium	255271	1371146	Medium	256458	1377991	Medium	261897	1406820
Coarse	190737	1023838	Coarse	192319	1033189	Coarse	190737	1023838

Ensuring a dependable mesh is crucial for obtaining precise outcomes. To ensure the robustness of the results, a sensitivity analysis for meshing was conducted. Fig. 3(a-c) illustrate the mesh configurations employed for the BI-WEHS model with the specified parameters: Three distinct meshes were assessed: coarse, medium, and fine. Ensuring mesh independence requires the convergence of results to approximately equal values. Table 2 provides details on mesh sizes for the three parameters. In regions proximate to walls, high solution gradients require precise calculations, which are crucial for the success of the simulation. Given the criticality of forces on the aerofoils in simulations, a meticulous approach to near-wall treatment is vital. This involves addressing the viscous sublayer to achieve a y+ value of approximately 1 at the initial grid cell near the wall. As demonstrated in Fig. 3(a-c), mesh refinement is strategically implemented around the aerofoil and rod to ensure a $y+ < 1$ all through the whole simulations.

The reliability of the CFD method was analyzed based on previous studies (Maalouly et al., 2022; Jaohindy et al., 2013; Wang and Chen, 2022). In summarising the mentioned studies, mesh sensitivity analyses were conducted to evaluate the impact of varying mesh resolutions (fine, medium, and coarse) on accuracy and computational efficiency. The fine mesh offered high detail and accuracy but demanded substantial computational resources, while the medium mesh achieved a balance between accuracy and efficiency, capturing essential aerodynamic features. The utilisation of a coarse mesh aimed to enhance computational efficiency, although at the cost of losing certain levels of detail. While the first study Maalouly et al (Maalouly et al., 2022). specifically detailed both mesh and time step sensitivity analyses, the others incorporated mesh sensitivity to accurately capture aerodynamic forces in varying rotor geometries and predict aerodynamic damping and vortex-induced vibrations. However, these were not clearly outlined in the respective papers, showcasing variations in the level of detail and emphasis on sensitivity analyses across the studies.

To evaluate the dynamic mesh behavior, the mesh distribution can be sampled at specific locations along the aerofoil surface at different instances during the simulation. At each angle of attack, the mesh distribution can be examined at key positions, such as the leading edge, mid-chord, and trailing edge of the aerofoil. These samples can provide insights into how the mesh displaces or oscillates and adapts to capture the changing flow conditions around the aerofoil throughout the pitching motion. As shown in Fig. 4(a-d), areas of high mesh density near the leading edge and trailing edge of the aerofoil indicate regions of intense flow separation or vorticity formation, potentially influencing lift and drag characteristics. Conversely, regions of lower mesh density, particularly downstream of the aerofoil, may suggest smoother flow conditions with reduced aerodynamic effects. Additionally, observing how the mesh evolves over time during dynamic simulations can reveal the transient behavior of lift and drag forces, highlighting fluctuations or oscillations in aerodynamic performance as the aerofoil moves through different angles of attack. Overall, analyzing mesh distribution provides valuable diagnostic information for understanding the complex interplay between flow dynamics, mesh behavior, and aerodynamic forces acting on the aerofoil.

Moreover, in near-wall regions where solution gradients are particularly high, ensuring accurate calculations is imperative for the success of the simulation. Given the critical role of forces on the aerofoil, near-wall treatment becomes essential. Resolving the viscous sublayer and employing mesh inflation around the aerofoil and rod ensures a smooth transition in mesh resolution, guaranteeing accuracy throughout all simulations. Through addressing these complexities in mesh refinement and near-wall treatment, the simulation framework maintains fidelity in capturing aerodynamic phenomena, ultimately enhancing the reliability and trustworthiness of the computational results.

Examining samples of results of mesh distribution at various positions of the aerofoil offers valuable insights into the dynamic behavior of

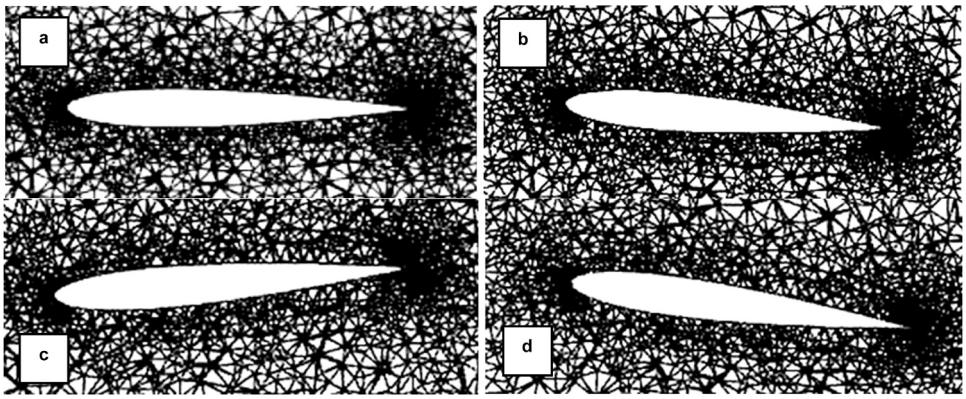

Fig. 4. Samples of results of mesh distribution at different positions of the aerofoil for dynamic mesh behavior in different angles (a) 0 degree (b) 5 degrees (c) −10 degrees (d) 10 degrees.

the mesh, particularly concerning lift and drag forces acting on the aerofoil. Through analyzing the mesh distribution, one can observe how the mesh adapts and deforms in response to changes in the flow field around the aerofoil. Specifically, variations in mesh density and structure can provide indications of regions where the flow is highly complex or where significant aerodynamic forces are exerted.

3.2.2. Mesh sensitivity analysis

To validate the dynamic mesh behavior, it is imperative to analyze the mesh distribution at various positions of the aerofoil throughout the simulation. Fig. 4 showcases the aerofoil response to pitching motions at freestream velocities of 3 m/s, 6 m/s, and 9 m/s, alongside different angles of attack (0°, 5°, 10°, and 15°). Employing a comprehensive meshing approach in dynamic mesh simulations ensures efficient capture of flow dynamics while upholding computational accuracy. Tetrahedral meshing around the aerofoil guarantees precise boundary layer resolution and dependable turbulence modeling, ensuring grid independence for an accurate representation of aerodynamic behavior. A mesh sensitivity study was conducted, varying the mesh size, and assessing the scheme convergence. This sensitivity analysis encompassed three parameters, including the NACA 0012 aerofoil integrated into three distinct roof configurations including flat, pitched, and curved structures. It is crucial for the mesh sensitivity test to consider lift coefficients of the aerofoil at specific angles of attack (e.g., 10°).

The investigation evaluates various mesh resolutions such as fine, medium, and coarse, and their effects on result precision and computational expenses within the simulation framework. Fine meshes are known for their complex detail and precision, which offer a nuanced understanding of the studied phenomena. However, this advantage accompanies significantly higher computational resource requirements. Conversely, coarse meshes prioritize computational efficiency by sacrificing some detail, yet they offer broader insights into overall system behavior.

Fig. 5(a-c) play a pivotal role in this analysis, providing a comparative assessment of the aerofoil lift coefficient across different mesh resolutions and parameters. Results unveil a consistent evolution in wind energy capture technology with medium and fine meshes, indicating accurate capture of system dynamics. However, disparities emerge with coarse meshes, suggesting inadequate representation of airflow complexities around the aerofoil. Furthermore, the evolution of results with mesh refinement, as depicted in Fig. 5 highlights the importance of attaining optimal mesh resolution in numerical simulations. While mesh refinement enhances accuracy, it also escalates computational costs. In this context, the medium mesh, offering identical results to the fine mesh but with lower computational burden was chosen for all simulations. This decision ensures a balance between accuracy and computational efficiency, maximizing the utility of computational resources.

Considering computational expenditure, employing a fine mesh entails a significant time investment for simulation completion. Thus, the medium mesh was selected to strike a balance, delivering satisfactory CFD quality without overburdening computational resources. Specifically, the fine mesh required 20 hours, the medium mesh 12 hours, and the coarse mesh 9 hours of processing time on a PC equipped with a 6-core processor.

3.2.3. Time sensitivity analysis

The time sensitivity assessment was carried out to examine the effect of time step variations on transient simulations that studied the velocity magnitude at the leading edge of a NACA 0012 aerofoil. The analysis was performed within the context of three different building roof shapes: flat, pitched, and curved. Two-time step sizes (0.035 s and 0.03 s) were used, aiming to maintain a Courant–Friedrichs–Lewy (CFL) number below 1. As shown in Fig. 5(a-c), the sensitivity analysis provided valuable insights into how variations in input parameters, specifically time steps, influenced the output, facilitating the identification of the optimal parameter value. In essence, reaching numerical stability at almost 1(t) s flow time in computational fluid dynamics (CFD) simulations for the two parameters under 0.035 s and 0.03 s time steps, which signify efficient convergence, suitable numerical methods, and time step sizes, indicating the physical significance of the results. Table 3 provides a summary of the parameters investigated in the time sensitivity analysis conducted for this study. This not only enhances computational efficiency and emphasises parameter sensitivity but also underlines the importance of validating results against real-world data to ensure their accuracy and applicability to the studied physical system. Consequently, a time step of 0.035 s was adopted for subsequent simulations, yielding computational cost and time savings.

The CFL number is a dimensionless parameter used to determine the stability of numerical simulations, particularly in fluid dynamics. It calculated as the product of the time step size (Δt), the velocity of the flow (V), and the reciprocal of the characteristic length scale (L), divided by the kinematic viscosity (v). The Eq. (3) (ANSYS, 2009) for CFL number (CFL) is:

$$CFL = \frac{V \bullet \Delta t}{L \bullet v} \tag{3}$$

The CFL number was calculated for each time step using the formula: CFL = (velocity × time step) / grid spacing. This Table 3 allows for the analysis of how changing the time step affects the CFL number, which is critical for ensuring numerical stability and accuracy in simulations. Table 3 shows the sensitivity analysis of time steps for two different values including 0.035 and 0.03 with a constant velocity of 3 m/s.

In the current Computational Fluid Dynamics (CFD) study, both mesh and time step sensitivity analyses are pivotal for optimising accuracy and efficiency. The mesh sensitivity analysis ensures that the simulations accurately represent complex flow interactions around an

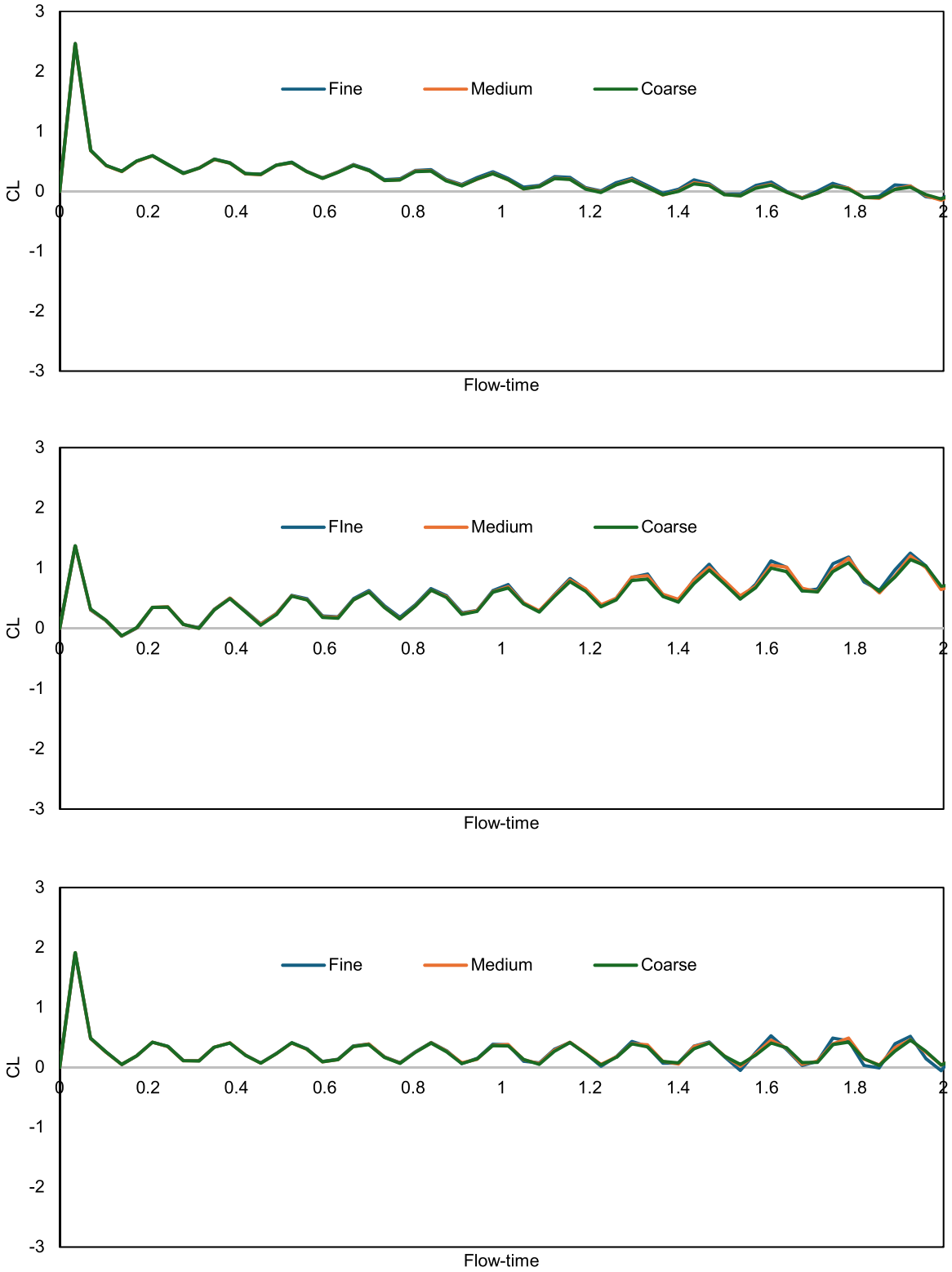

Fig. 5. Mesh grid sensitivity analysis for the lift coefficient of NACA 0012 installed into the (a) flat (b) pitched, and (c) curved roof structure.

Table 3
Time steps sensitivity analysis.

Time step (s)	Velocity (m/s)	Grid Spacing (m) for CFL =1
0.035	3	0.105
0.03	3	0.09

aerofoil and various building roof structures. It aids in determining the ideal mesh resolution, striking a balance between computational efficiency and result precision. Similarly, the time step sensitivity analysis is essential for maintaining simulation stability during transient behaviour, crucial in capturing the evolving flow patterns. It enables the selection of appropriate time steps that neither sacrifice accuracy nor overstrain computational resources. Overall, these sensitivity analyses

are fundamental in guiding parameter choices and ensuring dependable insights into aerofoil behaviour in different roof shapes, enhancing the overall quality and success of the study.

Fig. 6 show the choice of time step in the sensitivity analysis not only affects computational efficiency but also has implications for the accuracy of aerodynamic parameters such as lift coefficient (CL) of the aerofoil. In the context of the study, the selection of a time step directly impacts the temporal resolution of the simulation, influencing how well the aerodynamic forces acting on the aerofoil are captured over time. A finer time step, such as 0.03, allows for more frequent updates of the flow field and aerodynamic forces acting on the aerofoil throughout the simulation. This finer resolution can potentially result in more accurate predictions of the lift coefficients, especially in capturing transient phenomena or rapid changes in flow conditions. However, this increased temporal resolution comes at the cost of higher computational demands. On the other hand, a coarser time step, such as 0.035, provides less frequent updates of the flow field and aerodynamic forces. While this may lead to slightly reduced accuracy in capturing rapid changes, it also reduces computational time, making it a more efficient choice for simulations where computational resources are limited.

Overall, this approach integrates multiple analyses to make informed decisions about simulation parameters. Through carefully considering how variations in time step affect aerodynamic parameters and coordinating this with the findings of the mesh sensitivity analysis, the

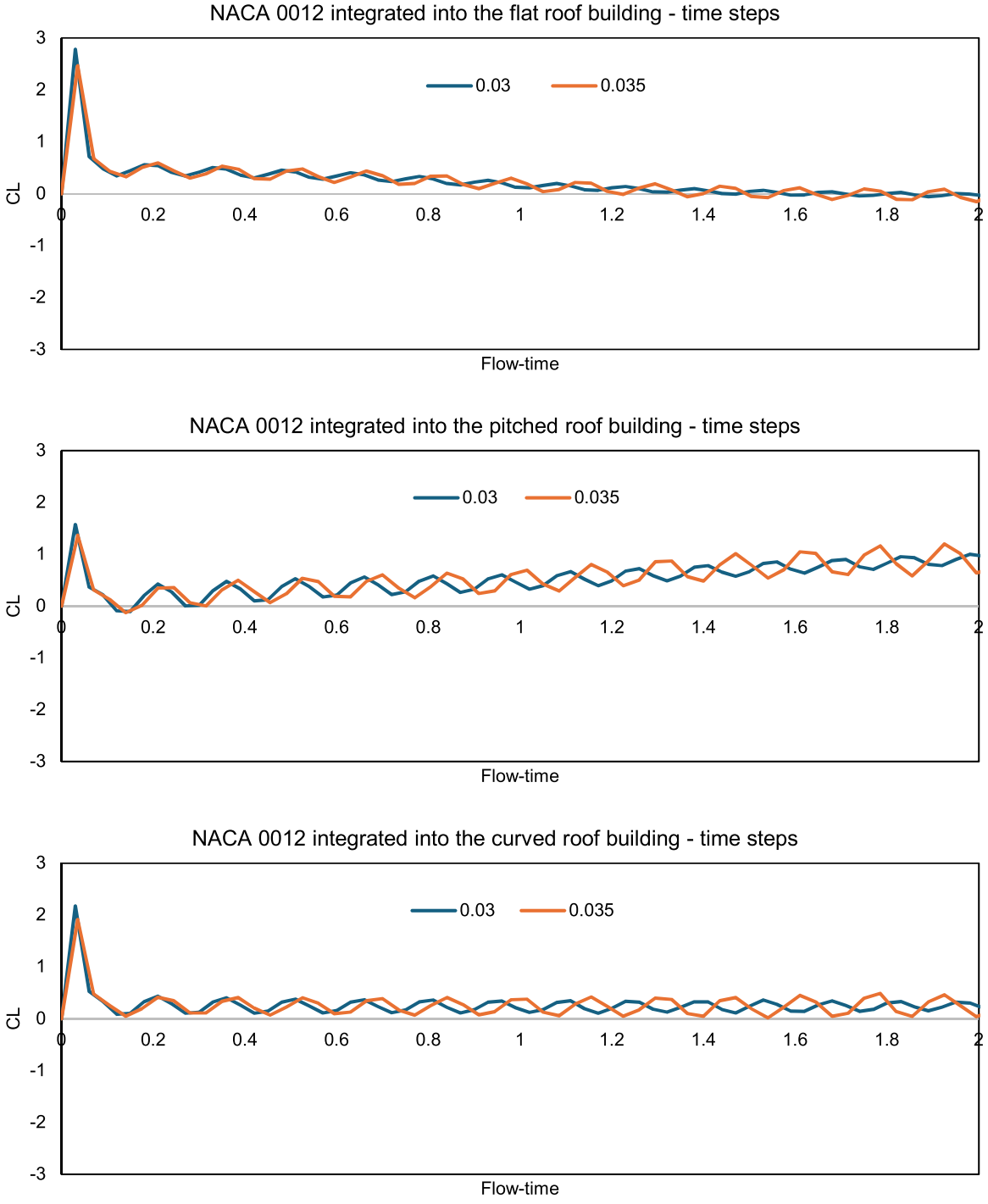

Fig. 6. Time sensitivity analysis for the lift coefficient of NACA 0012 installed into the (a) flat (b) pitched, and (c) curved roof structure.

confidence with selecting the optimal time step that balances accuracy, reliability, and computational efficiency in predicting the lift coefficients of the aerofoil.

3.3. CFD set up and boundary conditions

The simulation used a 3D unsteady Reynolds-averaged Navier-Stokes (URANS) equation model along with momentum and continuity equations to analyze the dynamic behaviour of the proposed Building-Integrated Wind Energy Harvesting System (BI-WEHS). In Table 4, it demonstrates the CFD model set up and boundary conditions for analysing the dynamic behaviour of the proposed design of BI-WEHS. The inlet velocities were set to 3, 6, and 9 m/s with wall boundary conditions on the top boundary. For the pressure-based, the transient model was used for this simulation while considering the gravitational forces. For an oscillating aerofoil with constant 850 (n-m/rad) under 1 degree of freedom (1-DOF) rotational rigid body motion in ANSYS Fluent, it means that the simulation is modelling the aerofoil motion in a fluid flow environment where the aerofoil is subjected to rotational oscillations around a fixed axis. The spring constant represents the stiffness of the rotational spring system, indicating how resistant the system is to rotational displacement. The selection of a constant 850 (n-m/rad) is supported by relevant studies (Abdizadeh et al., 2022; Chai et al., 2021b; Gao et al., 2022; Menon and Mittal, 2019; Sazesh and Shams, 2017; Rad and Khoshnevis, 2023) investigating various aspects of oscillating aerofoil systems. These studies indicate that this specific spring constant optimizes stability, controls oscillations effectively, and regulates dynamic response. Its importance lies in providing predictable and controlled aerofoil movements, preventing undesirable oscillations, and contributing to enhanced aerodynamic performance, stability, and control under different flow conditions.

The application of constant 850 (n-m/rad) m spring constant in the simulation of oscillating aerofoil systems, supported by studies in the field, ensures enhanced stability, precise control of oscillations, and regulation of dynamic response. This specific spring constant has been chosen to provide predictable and controlled aerofoil movements, effectively preventing undesired oscillations. Moreover, the utilization of a 1-degree-of-freedom setup, focusing on rotational motion typically around the pitch axis, simplifies the simulation while enabling a comprehensive analysis of the aerofoil behaviour under varying fluid forces. The incorporation of a dynamic mesh approach further enhances accuracy by facilitating detailed examination of aerofoil deformations and forces such as lift and drag. This methodology, combined with a 1-DOF solver and rigorous grid quality assessment techniques, contributes to improved stability, control, and accuracy in aerodynamic simulations, thereby advancing the optimization of aerofoil design and performance.

The 1-DOF setup, focusing on rotational motion typically around the pitch axis, simplifies the simulation while enabling a comprehensive analysis of the aerofoil behaviour under different fluid forces. Additionally, the dynamic mesh approach enhances accuracy by facilitating detailed examination of aerofoil deformations, lift, and drag forces. This methodology, combined with rigorous grid quality assessment techniques, contributes to improved stability, control, and accuracy in aerodynamic simulations, advancing aerofoil design optimization and performance. Moreover, the unsteady Computational Fluid Dynamics (CFD), determining convergence poses unique challenges due to time-varying solutions. In this study, the CFD results utilized the monitors, flow patterns, and residuals to assess convergence. Monitors track variations in outputs over time, ensuring expected behaviour or stabilization indicative of convergence. While the flow patterns were qualitatively assessed in terms of simulation sensibility, identifying irregularities. The residuals monitor iterative solution progress, with decreasing trends indicating convergence toward a periodic solution. In conclusion, navigating convergence in unsteady CFD simulations requires adaptability and a combination of specialized tools to ensure accurate and reliable results.

Moreover, the k-epsilon turbulence model and a 1 degree of freedom (1-DOF) dynamic mesh approach were applied for these simulations. The choice of wall treatment and corresponding y^+ values become crucial for accurately capturing the near-wall flow behaviour. The k-ε models with enhanced near-wall treatment were used. These models directly resolve the viscous sublayer and accurately capture the complex flow patterns occurring near the wall. For the oscillating NACA 0012 integrated into the building roof cases where the dimensionless wall distance y^+ is less than 1, low Reynolds number models were employed to ensure accurate representation of laminar or transitional flow phenomena near the wall. The model offered comprehensive understanding of flow behaviour in critical regions, enabling detailed analyses of aerofoil and building aerodynamic characteristics. This range is advised to ensure precise predictions of near-wall turbulence effects. By adhering to this range, the model can effectively capture the complex dynamics occurring close to the wall, thereby enhancing the accuracy of the predictions in computational fluid dynamics simulations. However, in simulations involving dynamic mesh motion, such as oscillating aerofoils, the near-wall flow behaviour can be highly complex and dynamic, requiring finer resolution near the wall. In such cases, especially when employing specific wall treatment models that demand very fine mesh resolution near the wall, y^+ values below 1 may be necessary to accurately capture the turbulent structures and shear effects close to the surface. This finer mesh resolution helps in better resolving the boundary layer and turbulent flow structures, which is essential for accurately predicting the aerodynamic forces acting on the oscillating aerofoil.

The selection of a 1-meter chord length and 1-meter span for an oscillating aerofoil integrated into a building roof structure is supported by findings from various studies focusing on wind energy harvesting systems. Roothaan et al (Roothaan et al., 2012). emphasize the importance of design parameters such as chord length and span in maximizing energy capture while minimizing the impact on surrounding structures and aesthetics, aligning with the concept of compact design for compatibility with urban environments. Similarly, Batay et al (Batay et al., 2024). explore blade dimensions to balance performance and structural integrity, suggesting that smaller chord lengths and spans optimize aerodynamic efficiency while maintaining stability. Robles-Ocampo (Hernandez-Estrada et al., 2021) provides insights into considerations for wind turbine tower design, potentially discussing optimal dimensions to withstand wind loads and ensure stability. Finally, Willis et al (Willis et al., 2018). offer a comprehensive review of wind energy research, including discussions on chord length and span optimization, supporting the use of a 1-meter chord length and 1-meter span for efficient energy capture. Overall, these studies provide a solid foundation for the selection of compact dimensions in wind energy systems, aligning with established principles and findings in the field.

For the freedom of movement of the aerofoil in this simulation, the axis of the rod was positioned at 0.25 m from the leading edge along the chord length. Remeshing-smoothing commands were implemented in the simulations. To analyze pitch motion, a one-degree of freedom (1-DOF) rotation solver with a center at 0.25 and along the z-axis was

Table 4
CFD model set up and boundary conditions.

Turbulence model	Standard K-epsilon
Algorithm	SIMPLE
Time	Unsteady state
Solver type	Pressure based
Discretisation Scheme	First order upwind
Turbulence model	Standard k-epsilon
Wall boundaries	Standard wall functions
Wall (Sides)	Wall (zero normal velocity and zero gradients)
Wall (Top)	Wall (zero normal velocity and zero gradients)
Fluid	Air
Inlet velocity (m/s) at UH	3 m/s, 6, m/s, and 9 m/s
Pressure outlet	0 Pa
Gravity (m/s^2)	-9.81

utilized, with a mass of 3.27 kg and a moment of inertia of 0.4 kg.m^2. The center of gravity was situated at 0.41 m along the chord length, with these values derived from the material properties of PVC foam as depicted in the DesignModeler CAD model of the NACA 0012 aerofoil profile.

3.4. Validation for oscillating NACA 0012 aerofoil

For the oscillating aerofoil, the current CFD results were compared against the study of Poirel et al (Poirel and Harris, 2008). The current CFD results were validated against the experimental data from the research of (Poirel and Harris, 2008). Fig. 7 shows the aerofoil test section and investigation of self-sustained oscillations of an oscillating aerofoil under pitch motion through wind tunnel experiments in the research of (Poirel and Harris, 2008). The design was replicated as a three-dimensional CFD model using the ANSYS Designmodeler to generate the computational grid. The aerofoil has a chord length of 0.156 m and a span length of 0.61 m, positioned within the tunnel with 7 mm between the wingtip and the top and bottom plates. In addition, a support rod with a diameter of 15 mm, located approximately one-quarter chord length (0.1c) from the leading edge, facilitates both pitch and heave motion of the aerofoil. The geometry comprises a wind tunnel domain with dimensions of 0.624 m (width) × 0.91 m (height) × 1.56 m (length), housing an aerofoil featuring a NACA 0012 aerofoil cross-section.

In the CFD study, the geometry was meshed in Ansys Meshing software using tetrahedral elements, resulting in 1,378,924 elements and 307,083 nodes in the computational domain. A dynamic mesh approach was employed to accommodate the aerofoil dynamic motion, with automatic mesh reconstruction using Remeshing and Smoothing commands to maintain mesh quality during updates. Grid quality assessment based on skewness, orthogonality, and aspect ratio yielded metrics indicating uniform element shapes (skewness of 0.30), reasonable alignment of grid lines with flow direction (orthogonality of 0.50), and moderately elongated elements (aspect ratio of 1.18), meeting criteria for accurate and reliable CFD simulations.

In the absence of wind tunnel experimental data from Poirel et al (Poirel and Harris, 2008)., validation of time steps was conducted through a series of analyses, including grid convergence, temporal convergence, and stability analysis. The grid convergence study systematically varied mesh resolution to determine an optimal size for accurate results and guide time step selection, while the temporal convergence study refined time step sizes to capture transient phenomena more precisely. Additionally, a stability analysis evaluated numerical stability through criteria such as the Courant–Friedrichs–Lewy (CFL) condition, ensuring stability while accurately representing physics. Despite the preference for experimental validation, these computational techniques provide confidence in the reliability and accuracy of the CFD simulations.

Moreover, the mesh employed in the computational simulations was meticulously selected to ensure accuracy and reliability in capturing the flow dynamics around the oscillating aerofoil. Although specific details regarding the mesh size and structure were absent from the experimental data, efforts were made to construct a mesh that sufficiently represented the geometry and boundary conditions of the wind tunnel experiments. The mesh refinement strategy aimed to resolve flow features near the aerofoil surface and effectively capture turbulent structures in the wake region. Despite the lack of information regarding the time step used in the simulations within the experimental data, the validation process focused on comparing computational results with experimental measurements to evaluate the model accuracy. The absence of specific numerical details regarding the time step did not undermine the validity of the validation process. Instead, the emphasis was placed on capturing overall trends and qualitative behaviour observed in the computational results, ensuring that the model accurately represented essential features and trends from the experimental data. Consequently, the computational model was deemed valid for the purpose of validation, notwithstanding the lack of specific numerical details such as the time step.

The experimental setup described in (Poirel and Harris, 2008) was a rigid aerofoil. In Poirel et al (Poirel and Harris, 2008)., two factors were indeed considered: the frequency of oscillations with a stiffness value of 0 and the aeroelastic natural frequency. However, it is essential to note that the focus of the current study was to validate the frequency of oscillations with a stiffness value of 0, aligning with the primary objective of investigating the dynamic behaviour of an oscillating aerofoil under pitch oscillation. This decision was made to maintain a clear and focused analysis. While both factors of frequency oscillation with 0 stiffness and aeroelastic natural frequency were considered in the referenced study by (Poirel and Harris, 2008), the validation efforts were directed towards assessing the specific aspect of frequency oscillations with 0 stiffness. This choice was made to rigorously validate the aerodynamic performance of the oscillating aerofoil in pitch motion, which was the primary focus of our investigation. Setting the stiffness value to 0 essentially renders the structure rigid, implying that it behaves as if it were completely compliant and does not offer any resistance to deformation.

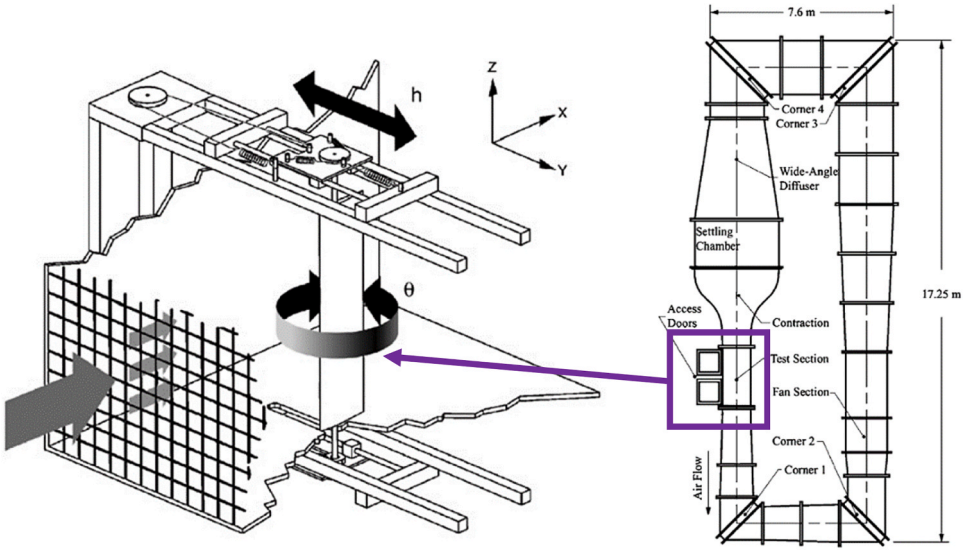

Fig. 7. Representation of the oscillating NACA0012 device in the wind tunnel (Poirel and Harris, 2008).

Therefore, by treating the structure as rigid in our analysis, the focus is solely on the aerodynamic aspects of the problem without accounting for any structural flexibility, aligning with the objectives of the current study.

This is followed by running CFD simulations by using dynamic mesh in one degree of freedom (1-DOF) solver. The aerofoil amount of mass and moment of inertia were also entered using the experimental data from (Poirel and Harris, 2008). For addressing the pitch rotational motion, a one Degree of Freedom (1-DOF) solver was employed to examine the dynamic behaviour of an oscillating aerofoil. The aerofoil possessed a mass of 0.771 kg, a moment of inertia of 0.00135 kg.m^2, a chord length of 0.156 m, and a span of 0.61 m. In addition, the wind tunnel solid blockage ratio, including the wing, rods, and plates, was maintained at 5% to minimize interference with the airflow during experimentation.

While acknowledging the importance of presenting time variation results and comparing them with reference data, it is crucial to note that the primary focus of the current manuscript differs. Specifically, the study primarily aimed to investigate the aerodynamic performance of the aerofoil under varying conditions of pitch oscillation frequencies, as detailed in (Poirel and Harris, 2008). Consequently, our analysis primarily focused on quantifying pitch oscillation frequencies in different wind speeds rather than temporal variations. This approach aligns with similar methodologies employed in other studies within our field. The current CFD approach of employing transient 1-DOF dynamic mesh CFD simulation with moving mesh aligns with the transient analyses conducted in several related studies. Alrawashdeh and Stathopoulos (Alrawashdeh and Stathopoulos, 2020) utilized transient simulations to assess wind loads on solar panels mounted on flat roofs, focusing on the effect of geometric scale. While in the study of (Yu-Hsien and Ahmad,

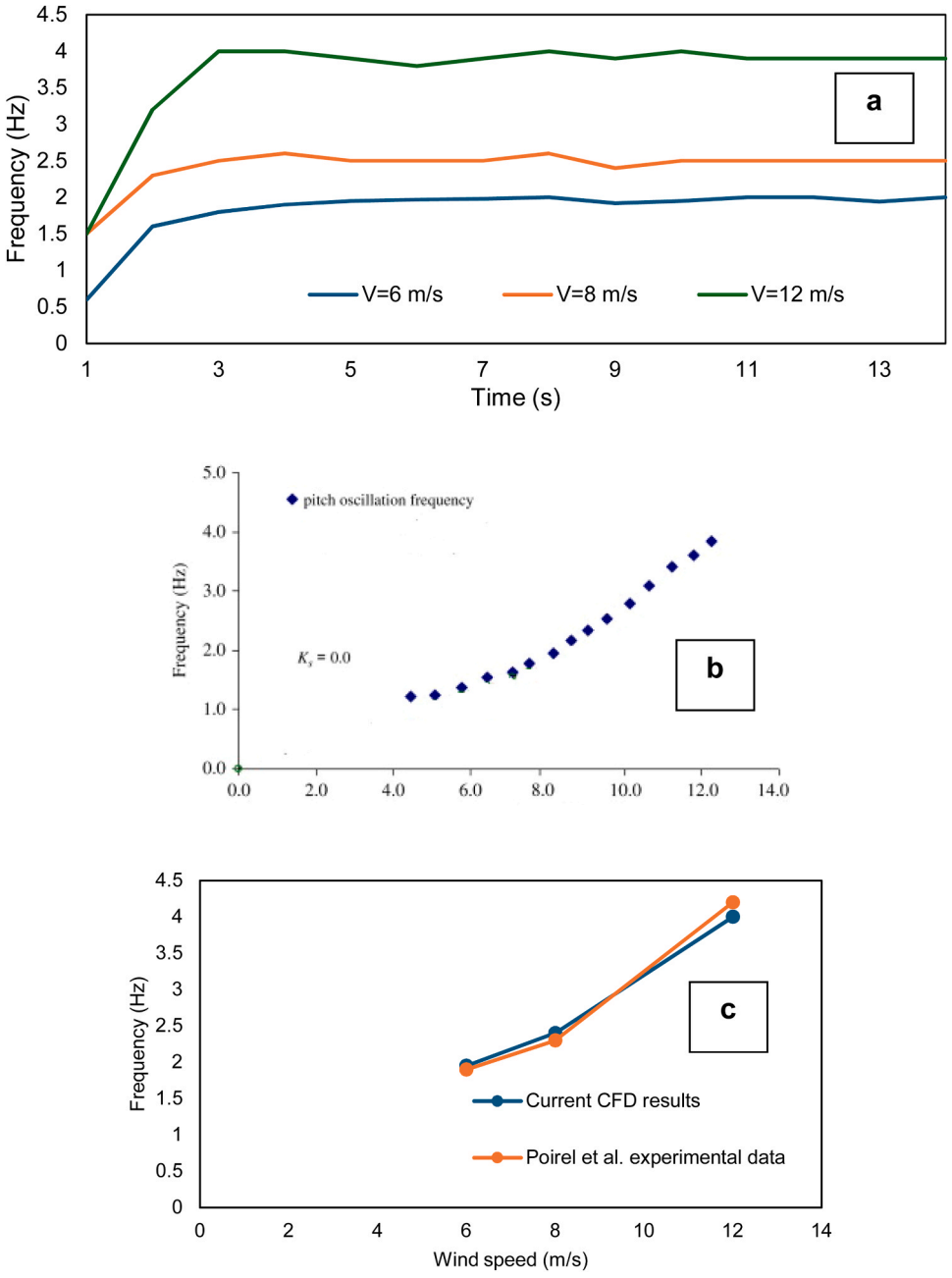

Fig. 8. Validation of (a) CFD results of frequency oscillation (b) plot diagram of frequency oscillation from the study of (Poirel and Harris, 2008), (c) comparative analysis of current CFD results against experimental data from the research of (Poirel and Harris, 2008).

2022), a transient analysis was conducted to study slamming wave loads on offshore wind turbine foundations generated by different types of breaking waves, emphasizing dynamic loading conditions. For the study of Abdessemed et al (Abdessemed et al., 2018)., the morphing aerofoils analysis using dynamic meshing, demonstrating the importance of adapting computational methods to capture complex aerodynamic phenomena over time. Despite differences in specific research objectives, the use of transient analyses in these studies reflects a shared emphasis on capturing dynamic behaviours and interactions with fluid flow. Therefore, the current study of using transient 1-DOF dynamic mesh CFD simulation with moving mesh is in alignment with similar methodologies employed in other studies within the field, emphasizing the importance of investigating aerodynamic performance under transient conditions.

The first-order upwind scheme is commonly utilized for the (k) turbulence kinetic energy and, correspondingly, (ε) turbulence dissipation rate in computational fluid dynamics (CFD) simulations due to its inherent numerical stability and robustness. This scheme employs a simple differencing approach that prioritizes stability over accuracy, making it well-suited for scenarios involving turbulent flows and dynamic mesh simulations where stability is paramount. Regarding the level of numerical diffusion involved, the first-order upwind scheme is characterized by a moderate level of numerical diffusion. While it sacrifices some accuracy compared to higher-order schemes, such as second-order upwind or central differencing, the first-order upwind scheme introduces a moderate amount of numerical diffusion to ensure stability, particularly in cases with rapidly changing flow conditions or mesh deformations. This numerical diffusion aids in damping out oscillations and maintaining stability, albeit at the expense of slightly smoothing out sharp gradients in the solution. Overall, the use of the first-order upwind scheme strikes a balance between stability, robustness, and computational efficiency, making it a practical choice for turbulence modelling in CFD simulations, especially in scenarios involving dynamic mesh motion and turbulent flows.

Fig. 8(a) presents the CFD results show the frequency oscillation under wind speeds of 6 m/s, 8 m/s, and 12 m/s over time. The highest frequency value, approximately 4 Hz, was observed under the 12 m/s wind speed condition, while the lowest frequency, around 1.5 Hz, occurred under the 6 m/s wind speed. Fig. 8(b) displays a plot diagram gathered from the study by Poirel et al (Poirel and Harris, 2008)., illustrating frequency oscillation data obtained from experimental measurements. Fig. 8(c) provides a comparative analysis between the frequency oscillation results from our numerical study and the experimental data sourced from (Poirel and Harris, 2008). Notably, the frequency values obtained from our CFD study closely match those reported in the experimental study. This consistency across different wind speeds indicates a low margin of error in our simulations compared to the experimental findings. Specifically, we observed a 2.6 % error for the 6 m/s wind speed, a 4.3 % error for the 8 m/s wind speed, and a 4.7 % error for the 12 m/s wind speed, highlighting the reliability of our simulation results.

The 3D CFD models were created using Ansys Design Modeler software and meshed with tetrahedral elements in Ansys Meshing software, resulting in a mesh comprising 10,000 elements and 42,000 nodes within the wind tunnel domain. Mesh quality evaluation, including skewness, orthogonality, and aspect ratio, met the required standards for precise CFD simulations. To adapt to the dynamic motion of the aerofoil, a dynamic mesh approach was employed, utilizing commands such as Remeshing and Smoothing to uphold mesh quality during updates. In the absence of experimental data, validation of time steps was conducted through complementary analyses, including grid convergence, temporal convergence, and stability analysis. These analyses systematically varied mesh resolution and time step sizes to assess solution sensitivity and transient behaviour, respectively. The stability analysis, crucial for ensuring numerical stability, evaluated criteria such as the Courant–Friedrichs–Lewy (CFL) condition to maintain stability while accurately representing the underlying physics. Despite the lack of wind tunnel experimental data, these computational techniques provided a robust framework for validating time steps, bolstering confidence in the reliability and accuracy of the CFD simulations.

For the validation of the velocity profile for the building roof, the study of Ntinas et al (Ntinas and Zhang, 2014). was considered. The geometry was initially designed using Ansys Design Modeler software and subsequently implemented in Ansys Meshing software to generate the computational grid. The geometry comprises a wind tunnel domain with dimensions of 0.5 m (width) × 0.5 m (height) × 6.91 m (length), housing a curved roof building. The curved roof building has a length of 0.5 m x 0.01184 m x 0.063 m. Similar dimensions were used for the width, height, and length for the pitched and flat roof building. Further details can be found in the study of Ntinas et al (Ntinas and Zhang, 2014). Fig. 9 shows the current CFD results that were validated against the experimental data and numerical simulations presented in Ntinas et al (Ntinas and Zhang, 2014). study, providing further support for the use of wall boundary conditions. Through recreating similar dimensions and roof shapes as investigated by Ntinas et al (Ntinas and Zhang, 2014)., the CFD simulations in the current study were compared with the experimental data and numerical simulations from Ntinas et al (Ntinas and Zhang, 2014). study. The level of agreement observed between the current CFD results, experimental data, and previous numerical simulations reinforces the accuracy and reliability of the computational model in simulating airflow patterns around obstacles with arched and pitched roofs. Thus, through validating the current CFD results against Ntinas et al (Ntinas and Zhang, 2014). study, the use of wall boundary conditions on the top boundary in simulations is justified, as it effectively simulates real-world airflow patterns, providing confidence in the numerical simulations conducted in the current study. In addition, the utilization of wall boundary conditions on the top boundary in this simulation aligns with the experimental setup observed in the study by Ntinas et al (Ntinas and Zhang, 2014).

The investigation of airflow patterns around obstacles with various roof shapes, Ntinas et al (Ntinas and Zhang, 2014). conducted wind tunnel experiments with physical surfaces or obstacles at the top boundary. Through implementing wall boundary conditions in simulations, the airflow interaction with these physical barriers, ensuring that our simulations capture realistic airflow behavior around obstacles, consistent with experimental observations were replicated. Moreover, the wall boundary conditions were commonly utilized in CFD simulations to model solid surfaces, providing a realistic representation of the airflow interaction with physical boundaries. This approach allows for the accurate simulation of flow phenomena near obstacles, crucial for understanding the aerodynamic effects of structures such as buildings or roof shapes. Therefore, using wall boundary conditions on the top boundary in simulations is a justified approach as it effectively mirrors the experimental conditions observed by Ntinas et al (Ntinas and Zhang, 2014).

4. Results and discussion

To investigate the impacts of force and static pressure on self-induced oscillations of a pitching aerofoil, the study involves an examination of velocity magnitude and pressure contours obtained from Unsteady Reynolds-Averaged Navier-Stokes (URANS) simulations at various wind velocities, including 3 m/s, 6 m/s, and 9 m/s. The decision to focus on lower wind speeds of 3 m/s, 6 m/s, and 9 m/s in the CFD study was driven by the specific context of urban flows, where lower wind speeds are commonly observed. This choice was made to align the simulation conditions with scenarios typically encountered in urban environments, where airflow dynamics can be characterized by relatively lower wind speeds. This rationale was indeed explained clearly in the article, where we provided justification for the selection of wind speeds and discussed how they correspond to real-world conditions, particularly in urban settings. Therefore, while the experimental tests

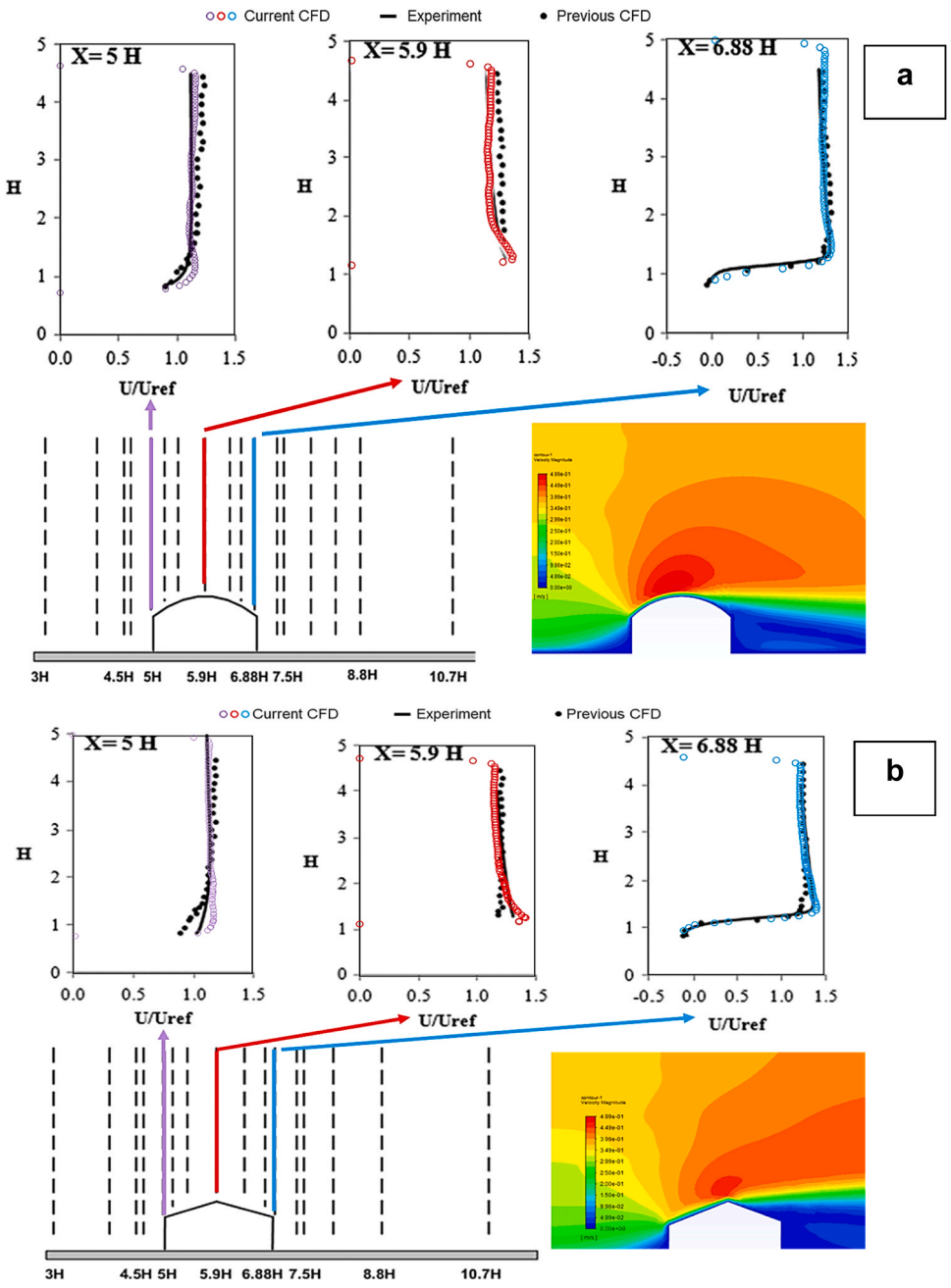

Fig. 9. Comparative analysis of CFD results, experimental data, and previous CFD results (Ntinas and Zhang, 2014) for averaged steam-wise velocity around the (a) curved and (b) pitched roof building.

may have covered a broader range of wind speeds, our focus on lower wind speeds in the CFD study was deliberate and appropriate for the urban flow context being examined.

The aim is to assess the potential of the NACA 0012 oscillating aerofoil integrated into building roof for wind energy capture. This assessment involves the application of the dynamic mesh method in ANSYS Fluent, employing consistent boundary conditions and dynamic mesh settings across three distinct scenarios: the installation of the NACA 0012 aerofoil on flat, pitched, and curved building roof structures, while simultaneously varying wind speed and spring constant. The investigation employs different wind speeds to assess the influence of installing the oscillating aerofoil on these varying roof shapes.

4.1. Velocity magnitude and static pressure distribution

The research investigated the velocity magnitude and static pressure distribution for three distinct design configurations: oscillating NACA 0012 aerofoils integrated into flat, pitched, and curved roof buildings, each subjected to wind speeds of 3 m/s, 6 m/s, and 9 m/s. By examining contours, patterns of wind flow surrounding the aerofoils integrated into the building roofs were visualized. This visualization was instrumental in optimizing various aspects of aerofoil design, placement, or the implementation of additional control systems, all aimed at enhancing the efficiency of wind energy capture.

4.1.1. NACA 0012 integrated into the flat roof

When investigating an oscillating aerofoil under pitch motion, aerodynamic characteristics can be analyzed by examining velocity

magnitude and static pressure contours. Velocity magnitude contours provide insights into the airflow patterns around the aerofoil, revealing regions of high and low velocity and indicating areas of separation or attachment. These contours can support in identifying regions of flow acceleration or deceleration, which are crucial for understanding lift and drag forces acting on the aerofoil. Moreover, static pressure contours illustrate pressure distribution on the surface of the aerofoil, showing areas of high and low pressure. Through analyzing these contours, one can assess lift and drag distributions along the aerofoil surface, as well as identify locations of potential flow separation or stall. Both the velocity magnitude and static pressure contours provide valuable information for evaluating the aerodynamic performance and behaviour of the oscillating aerofoil under pitch motion, aiding in the design and optimization of such systems for various applications. The last cycle of oscillation was only captured for the velocity magnitude and static pressure contours, as it shows the most up-to-date information about the flow field before it repeats again. Also, this approach can provide a clearer and more concise representation of the velocity and pressure distributions surrounding the aerofoil during its periodic motion.

The dimensions of the building mentioned are 6 m x 6.6 m x 6 m. Videos 1, 2 and 3 show the apparent discrepancy in building dimensions as compared to Fig. 2 is due to the perspective difference in the video representation. In addition, it is only showing a cross sectional view of the building. The video aims to provide a dynamic visualization of the airflow around the building and the oscillating aerofoil, necessitating a different angle and perspective that might not exactly match the static cross-sectional view in Fig. 2.

Supplementary material related to this article can be found online at doi:10.1016/j.egyr.2024.04.022.

Video 1 demonstrates the velocity magnitude contours for the integration of an oscillating NACA 0012 aerofoil into a flat roof building to harness wind energy. In video 1, the airflow distribution above and around the aerofoil reveals significant observations. The video highlights the occurrence of a wind shear effect when the wind interacts with the edge of the flat roof building. This effect redirects the wind flow upwards, away from the aerofoil, instead of allowing it to directly impact the aerofoil. Wind shear is known to diminish the efficiency of wind energy harvesting systems by reducing the available wind energy for conversion. In addition, the video illustrates a substantial recirculation of the wind flow surrounding the aerofoil. This recirculation generates turbulent airflow patterns, which are detrimental to efficient energy harvesting. Turbulence disrupts the smooth operation of wind energy harvesting systems and decreases overall efficiency.

The presence of wind shear and recirculation suggests that the building roof shape and placement of the aerofoil may not be optimized for maximizing energy harvesting. To improve efficiency, it is necessary to reconsider the placement of the aerofoil relative to the building and explore design modifications to mitigate the effects of wind shear and turbulence. Efficient energy harvesting from wind requires meticulous consideration of aerodynamic design principles. This encompasses not only the design of the aerofoil itself but also its integration into the surrounding environment. Factors such as building shape, nearby obstacles, and prevailing wind patterns must be carefully evaluated to extract maximum energy. In conclusion, while the integration of an oscillating NACA 0012 aerofoil into a flat roof building holds promise for wind energy harvesting, the observed wind shear and recirculation underline the importance of thoughtful design and optimization to maximize efficiency.

In Fig. 10 (a-b), the velocity magnitude and static pressure are focused on the oscillating NACA aerofoil. In the scenario of a NACA 0012 integrated into the flat roof building at a wind speed of 3 m/s, the airflow is characterized by relatively gentle conditions, resulting in minimal lift and drag forces on the oscillating NACA 0012 aerofoil. Flow separation from the upper surface of the aerofoil occur at lower angles of attack due to the smoother flow conditions. With an increase in wind speed to 6 m/s, airflow becomes more active, leading to higher dynamic pressure and increased aerodynamic forces on the aerofoil, as shown in Fig.10 (c-d). At this speed, flow separation from the upper surface occurs

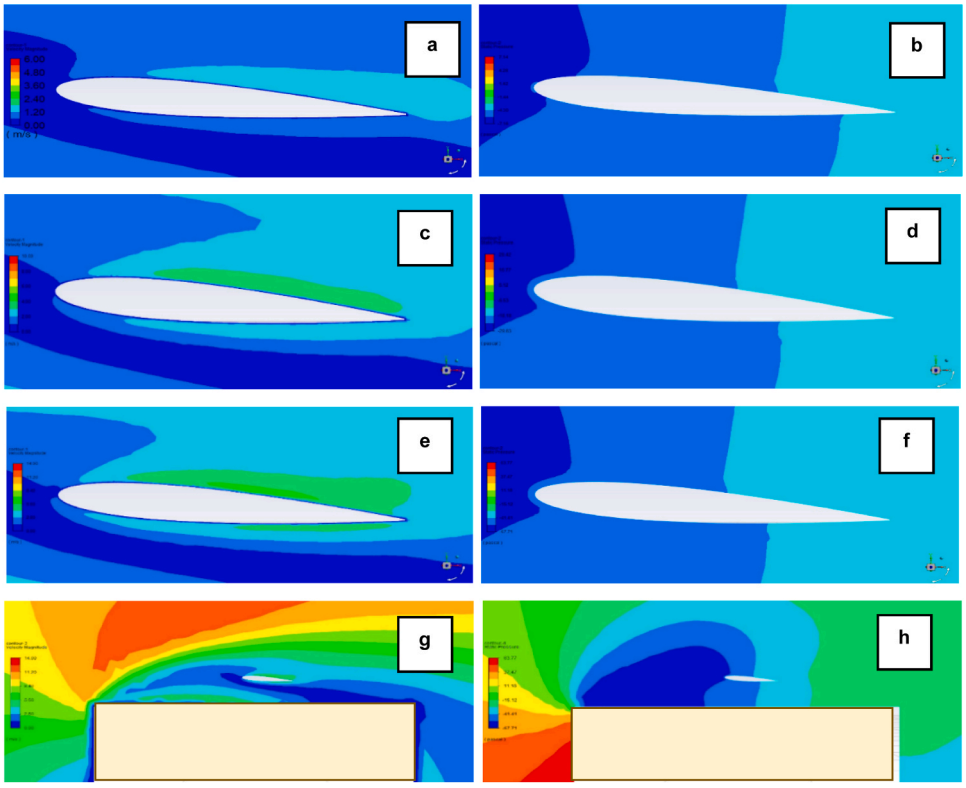

Fig. 10. Contours representing velocity magnitude under (a) 3 m/s, (c) 6 m/s, (e) 9 m/s, (g) integrated design of NACA 0012 and flat roof building under 3 m/s and static pressure under (b) 3 m/s, (d) 6 m/s, (f) 9 m/s, (h) integrated design of NACA 0012 and flat roof building under 3 m/s for last cycle oscillation.

at higher angles of attack compared to lower wind speeds. Furthermore, at 9 m/s wind speed, the airflow is even more active, resulting in further increased dynamic pressure and aerodynamic forces on the aerofoil. Flow separation occurs at even higher angles of attack, leading to enhanced lift and drag characteristics, as demonstrated in Fig.10 (e-f). At low 5-degree angle of attack, the flow exhibits smooth patterns with attached boundary layers, while moderate angle of attack reveals signs of flow separation near the trailing edge, evidenced by recirculation areas and pressure differentials.

Fig. 10 (g -h) show the velocity magnitude and static pressure for an oscillating NACA 0012 under pitch motions integrated into the flat roof building at 9 m/s. These results demonstrate the last cycle of oscillation not at fixed times as proposed.

In the scenarios ranging from 0 to 10 degrees angle of attack for an oscillating NACA 0012 aerofoil integrated into the flat roof building, various aerodynamic phenomena occur that affect lift and drag characteristics. At 0 degrees angle of attack, the airflow is relatively undisturbed, resulting in minimal lift and drag forces. As the angle of attack increases, typically around 5 degrees, the airflow begins to separate from the upper surface of the aerofoil near the leading edge. This separation occurs due to the increasing pressure difference between the upper and lower surfaces, leading to the development of a separation bubble and the onset of flow detachment. Consequently, the lift coefficient starts to increase as the airflow is redirected upwards, while the drag coefficient also rises due to increased flow separation.

At 10 degrees angle of attack, the separation of airflow from the upper surface of the aerofoil becomes more pronounced, extending further downstream along the chord. This separation bubble results in a larger region of flow detachment and turbulent wake formation, contributing to increased drag forces. The lift coefficient continues to rise, but at a diminishing rate due to the adverse effects of flow separation on lift generation. The trailing edge of the aerofoil experiences high levels of turbulence and vorticity, further exacerbating flow detachment and drag production.

Overall, as the angle of attack reaches 10 degrees, the contours reveal significant separation of airflow from the upper surface of the aerofoil. This separation profoundly impacts lift and drag characteristics, influencing the overall aerodynamic performance of the oscillating aerofoil integrated into the building roof structure.

4.1.2. Velocity magnitude and static pressure distribution for NACA 0012 integrated into the pitched roof

In Video 2, it shows velocity magnitude contours for the integration of an oscillating NACA 0012 aerofoil into a pitched roof building, presenting insights into wind energy harvesting dynamics. The video highlights several notable observations: Firstly, it is evident that the wind speed accelerates notably at the windward side of the pitched roof building. This acceleration presents a favourable condition for wind energy harvesting, as higher wind speeds generally correlate with increased energy generation potential. The design and placement of the aerofoil on the windward side effectively harness this accelerated wind flow to optimize energy conversion.

Moreover, a detachment phenomenon is observable at the leeward side of the building. This detachment signifies a disruption in the airflow, potentially creating a low-pressure zone that can further enhance energy harvesting efficiency. Through causing a detachment, the pitched roof building facilitates the creation of a favourable aerodynamic environment for energy extraction. However, it is essential to note that while the detachment at the leeward side offers benefits, it is only optimal for energy harvesting when the aerofoil is positioned on the windward side. This positioning ensures that the aerofoil captures the accelerated wind flow efficiently, maximizing energy generation. Conversely, a significant recirculation of airflow is observed at the leeward side of the building. This recirculation creates turbulent airflow patterns, which can hinder energy harvesting efficiency. Thus, positioning the aerofoil solely on the windward side is crucial to avoid the adverse effects of recirculation and maintain optimal energy extraction conditions.

In summary, Video 2 illustrates the advantageous aerodynamic effects of integrating an oscillating NACA 0012 aerofoil into a pitched roof building for wind energy harvesting. The accelerated wind speed at the windward side and the detachment phenomenon at the leeward side contribute to enhancing energy generation potential. However, careful consideration of aerofoil positioning is necessary to capitalize on these benefits while minimizing the impact of airflow recirculation on energy harvesting efficiency.

Supplementary material related to this article can be found online at doi:10.1016/j.egyr.2024.04.022.

Fig. 11 (a-h) demonstrate the velocity magnitude and static pressure for the oscillating NACA 0012 integrated into the pitched roof building under 3 m/s, 6 m/s, and 9 m/s airflow over the building exhibits relatively gentle conditions, resulting in minimal lift and drag forces on the aerofoil. Fig. 11 (a-b) show the flow separation occured at lower angles of attack due to smoother flow conditions. With an increase in wind speed to 6 m/s, airflow becomes more energetic, leading to higher dynamic pressure and increased aerodynamic forces on the aerofoil, as demonstrated in Fig. 11 (c-d) . Flow separation from the upper surface occured at higher angles of attack compared to lower wind speeds. Fig. 11 (e-h) shows the case for 9 m/s wind speed, the airflow is even more energetic, resulting in further increased dynamic pressure and aerodynamic forces on the aerofoil, causing flow separation at even higher angles of attack.

The current CFD analysis explores the aerodynamic behaviour of a NACA 0012 aerofoil across varying angles of attack (AoA) using computational fluid dynamics (CFD) simulations and contour analysis. Results indicate distinct flow patterns and pressure distributions at 10-degree AoA, the last cycle of oscillation. The result of high wind speed results against AoA, showed flow separation, which extended upstream along the aerofoil, resulting in increased turbulence and significant pressure gradients. Analysis identifies the critical AoA for flow separation and stall, while temporal evolution analysis uncovers transient phenomena like vortex shedding. The study underscores the effectiveness of CFD and contour analysis in understanding aerodynamic performance and determining optimal AoAs for lift maximization and drag minimization.

In the case of an oscillating aerofoil integrated into a pitched roof building, the aerodynamic behaviour becomes even more complex due to the dynamic interaction between the moving aerofoil and the surrounding flow field. The oscillating motion introduces unsteady flow phenomena, such as vortex shedding, which significantly affect the aerodynamic forces experienced by the aerofoil and the structural loads on the building. The integration of the aerofoil into the pitched roof alters the flow patterns around the building, potentially affecting the lift and drag characteristics of the aerofoil as well as the structural stability of the building. The Reynolds number of $\mathrm{Re} = 2.05x105$indicates a transitional flow regime, where both laminar and turbulent flow features are present, further complicating the analysis. Computational fluid dynamics (CFD) simulations coupled with dynamic analysis techniques are essential for accurately predicting the aerodynamic response of the oscillating aerofoil and its interaction with the pitched roof building. Wind tunnel testing can provide validation and refinement of the CFD results, ensuring the reliability of the aerodynamic and structural assessments. Overall, the integration of an oscillating aerofoil into a pitched roof building requires a comprehensive understanding of unsteady flow dynamics and structural response to optimize both aerodynamic performance and structural integrity.

4.1.3. NACA 0012 integrated into the curved roof

In Video 3, it shows the velocity magnitude contours for the integration of a NACA 0012 aerofoil into a curved roof building, shedding light on its impact on wind energy harvesting dynamics. The video reveals several significant observations: Firstly, it is evident that the wind

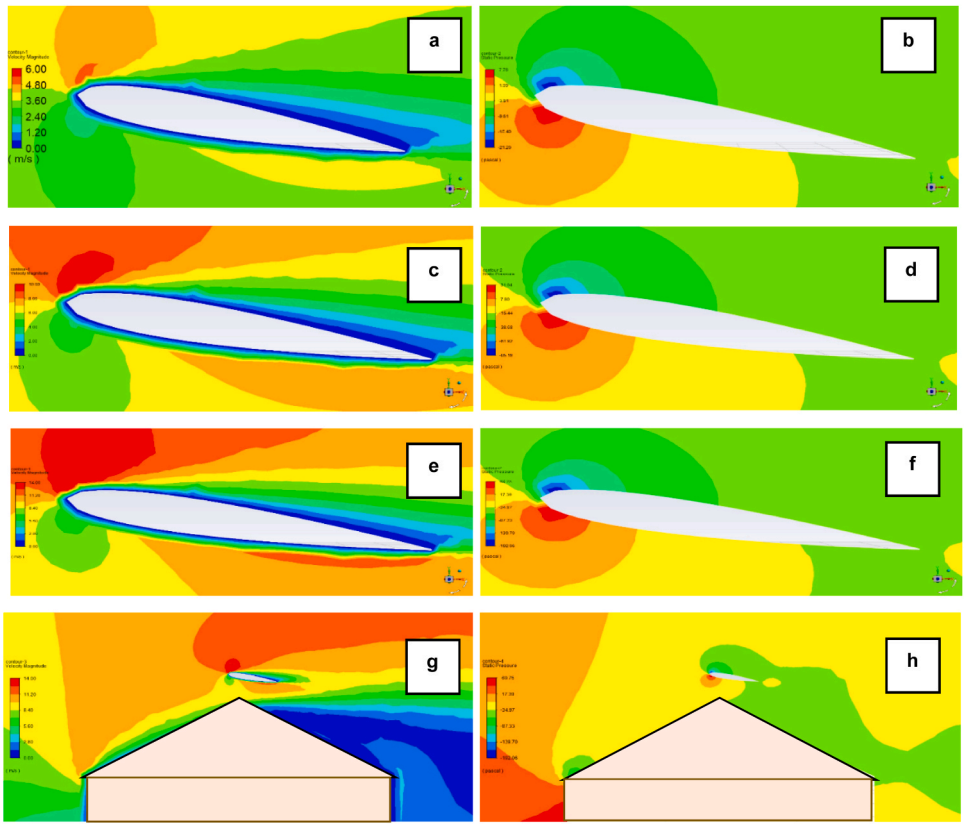

Fig. 11. Contours representing velocity magnitude under (a) 3 m/s, (c) 6 m/s, (e) 9 m/s, (g) integrated design of NACA 0012 and pitched roof building under 3 m/s and static pressure under (b) 3 m/s, (d) 6 m/s, (f) 9 m/s, (h) integrated design of NACA 0012 and pitched roof building under 3 m/s for last cycle oscillation.

flow tightly adheres to the curved roof building. This strong attachment of the wind flow to the building is highly advantageous for wind energy harvesting systems. The close adherence ensures efficient utilization of the wind kinetic energy, maximizing the potential for energy conversion. Moreover, the video demonstrates versatility in aerofoil placement within the curved roof building. Unlike the constraints observed with the NACA 0012 integrated into pitched roof buildings, where aerofoils are typically limited to the windward side, the curved roof design allows for more flexible placement options. This flexibility enables optimal positioning of the aerofoil to capitalize on prevailing wind directions and variations, enhancing energy harvesting efficiency.

Through exploring different placement options, the curved roof building offers greater adaptability in optimizing energy extraction. This adaptability is particularly valuable in environments with complex wind patterns or where wind direction fluctuates regularly. In contrast to pitched roof buildings, where aerofoil placement is often constrained to the windward side, the curved roof design provides opportunities for strategic placement throughout the structure. This flexibility allows for more effective utilization of available wind resources and maximizes energy generation potential.

In summary, Video 3 demonstrates the favourable aerodynamic characteristics of integrating a NACA 0012 aerofoil into a curved roof building for wind energy harvesting. The strong attachment of wind flow to the building and the flexibility in aerofoil placement contribute to optimizing energy extraction efficiency. This highlights the potential of curved roof designs to enhance wind energy harvesting systems by providing adaptable and efficient aerodynamic configurations.

Supplementary material related to this article can be found online at doi:10.1016/j.egyr.2024.04.022.

Fig. 12 (a-h) show the scenario of an oscillating NACA 0012 aerofoil curved roof building under 3 m/s, 6 m/s, and 9 m/s wind speed, airflow exhibit complex patterns due to the curved surfaces, resulting in moderate lift and drag forces on the aerofoil. Fig. 12 (a-b) shows the flow separation from the upper surface occur at intermediate angles of attack and high pressure at the leading edge on lower surface of the aerofoil at 3 m/s. With an increase in wind speed to 6 m/s, airflow becomes more active, leading to higher dynamic pressure and increased aerodynamic forces on the aerofoil. Flow separation from the upper surface occur at higher angles of attack compared to lower wind speeds, as shown in Fig. 12 (c-d). At 9 m/s wind speed, the airflow is even more active, resulting in further increased dynamic pressure and aerodynamic forces on the aerofoil, causing flow separation at even higher angles of attack, as demonstrated in Fig. 12 (e-h). These scenarios emphasize the importance of considering wind speed and roof shape in designing building-integrated wind energy systems to optimize aerodynamic performance.

At a Reynolds number of $\mathrm{Re} = 2.05x10\,5$, the flow around an aerofoil is suggestive of a transitional state between laminar and turbulent flow regimes, a critical range often observed in aerodynamic studies. This transitional flow presents a balance between the laminar and turbulent characteristics, with the potential for flow separation and increased turbulence. In the scenario of a semi-circular roof building with an aerofoil positioned at its center, the proximity of the aerofoil to the roof influences boundary layer development, potentially leading to flow separation on the aerofoil upper surface. In addition, the curved roof alters the local flow field, inducing flow separation near the aerofoil trailing edge due to adverse pressure gradients from the nearby surface. This setting offers a unique aerodynamic environment, demanding comprehensive analysis through computational fluid dynamics (CFD) simulations and wind tunnel testing to understand the complex flow patterns, optimize aerodynamic efficiency, and ensure structural stability. This Reynolds number aligns with literature findings on transitional flow behaviors around aerofoils, emphasizing the importance of accurate simulations and testing for practical applications.

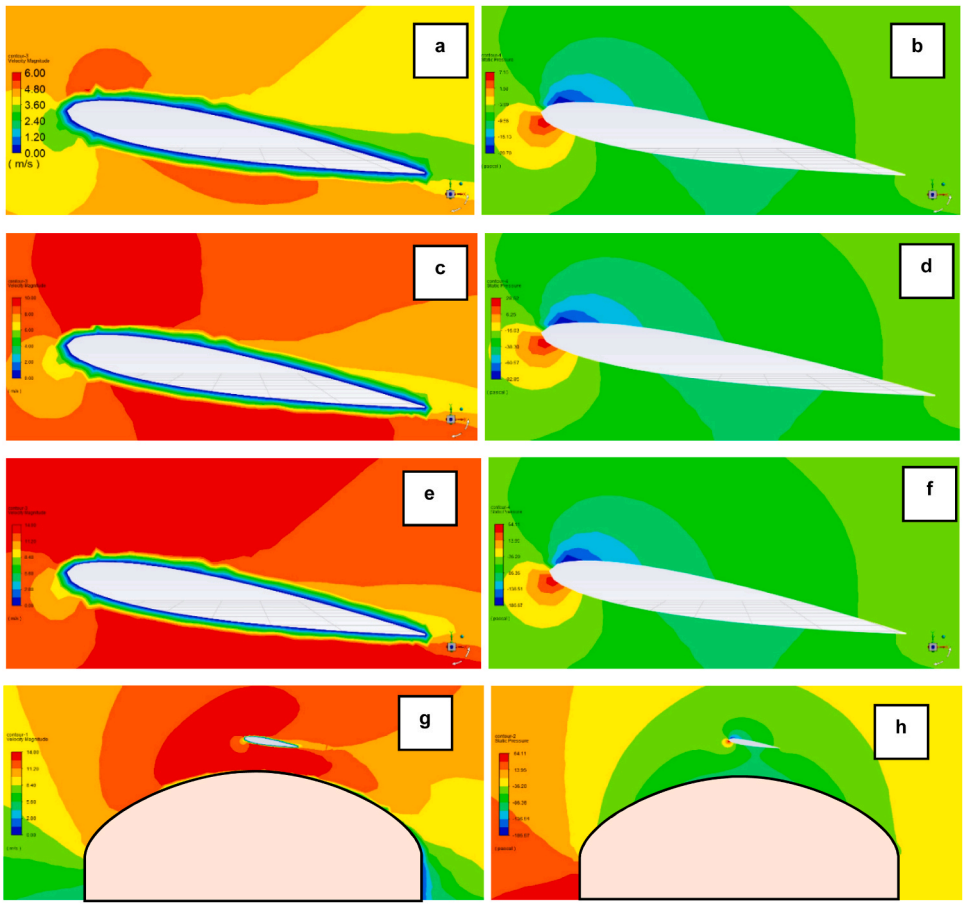

Fig. 12. Contours representing velocity magnitude under (a) 3 m/s, (c) 6 m/s, (e) 9 m/s, (g) integrated design of NACA 0012 and flat roof building under 3 m/s and static pressure under (b) 3 m/s, (d) 6 m/s, (f) 9 m/s, (h) integrated design of NACA 0012 and flat roof building under 3 m/s for last cycle oscillation.

4.1.4. Velocity profile surrounding the aerofoil integrated into the flat, pitched, and roof building

Fig. 13 (a and b) depict the velocity profiles surrounding the aerofoil at a 10-degree angle of attack when integrated into flat, pitched, and curved roof buildings. Fig. 13 (a) illustrates notable differences between the integration of the NACA 0012 aerofoil into flat and pitched roof structures. In the case of the flat roof building, wind speed acceleration was not observed due to wind shear, despite the aerofoil ideal placement. Instead, wind flow recirculation occurred around the aerofoil, resulting in an initial wind speed of 3 m/s decreasing to 1.7 m/s.

Conversely, integrating the NACA 0012 aerofoil into pitched and curved roof buildings led to wind speed enhancements, reaching 4.3 m/s for pitched roofs and 4.45 m/s at a 10-degree angle. Fig. 15(b), focusing on the velocity profile at the mid span of the aerofoil, reveals similar trends across cases. Notably, lower wind speeds are observed for the integration into flat roofs compared to pitched and curved roofs. Wind speed acceleration occurs prominently at the leading edge of the aerofoil in flat roof settings, while a decrease in acceleration is evident at the mid span due to roof shape and aerofoil placement.

In pitched roof configurations, wind speed acceleration is prominent on the windward side of the building, with wind flow detachment observed on the leeward side. Similar wind speed enhancements are observed for NACA 0012 integration into curved roof buildings, attributed to the shape of the roof and strong wind flow attachment. These findings align with studies in the literature, which emphasize the significant influence of roof geometry on wind flow patterns and the effectiveness of aerofoil integration in enhancing wind speeds in certain configurations.

4.2. Dynamic behaviour of the roof-integrated oscillating aerofoil energy harvester

This section examines the dynamic behaviour of an oscillating aerofoil wind energy harvesting system integrated into three different roof shapes, focusing on pitch angle, torque, and angular velocity to predict potential power output. A sensitivity analysis was conducted to assess the impacts of various factors such as wind speed, roof shapes, wind direction, and power spectral density across different frequencies.

4.2.1. Impact of wind speed

The influence of wind speed was evaluated based on the aerofoil pitch angle, torque, and angular velocity across three distinct design parameters: NACA 0012 integrated into flat, pitched, and curved roof buildings.

4.2.1.1. Aerofoil pitch angle. The dynamic variations of pitch angles for the NACA 0012 aerofoil integrated into flat, pitched, and curved roof buildings at different wind speeds (3 m/s, 6 m/s, and 9 m/s) are depicted in Fig. 14 (a-c). In Fig. 14 (a), it is evident that the NACA 0012 integrated into the curved roof building exhibited the highest pitch angle, peaking at 1.5 degrees at 10 seconds under 3 m/s wind speed. Conversely, the lowest pitch angle, approximately 0.5 degrees, was observed for the flat roof integration. This discrepancy is attributed to wind flow recirculation around the aerofoil due to the building roof shape and wind shear generated at the flat roof edge. Additionally, the 1-degree pitch angle observed for the pitched roof integration results from aerodynamic forces induced by the roof geometry.

At a wind speed of 6 m/s (Fig. 14 b), the NACA 0012 integrated into

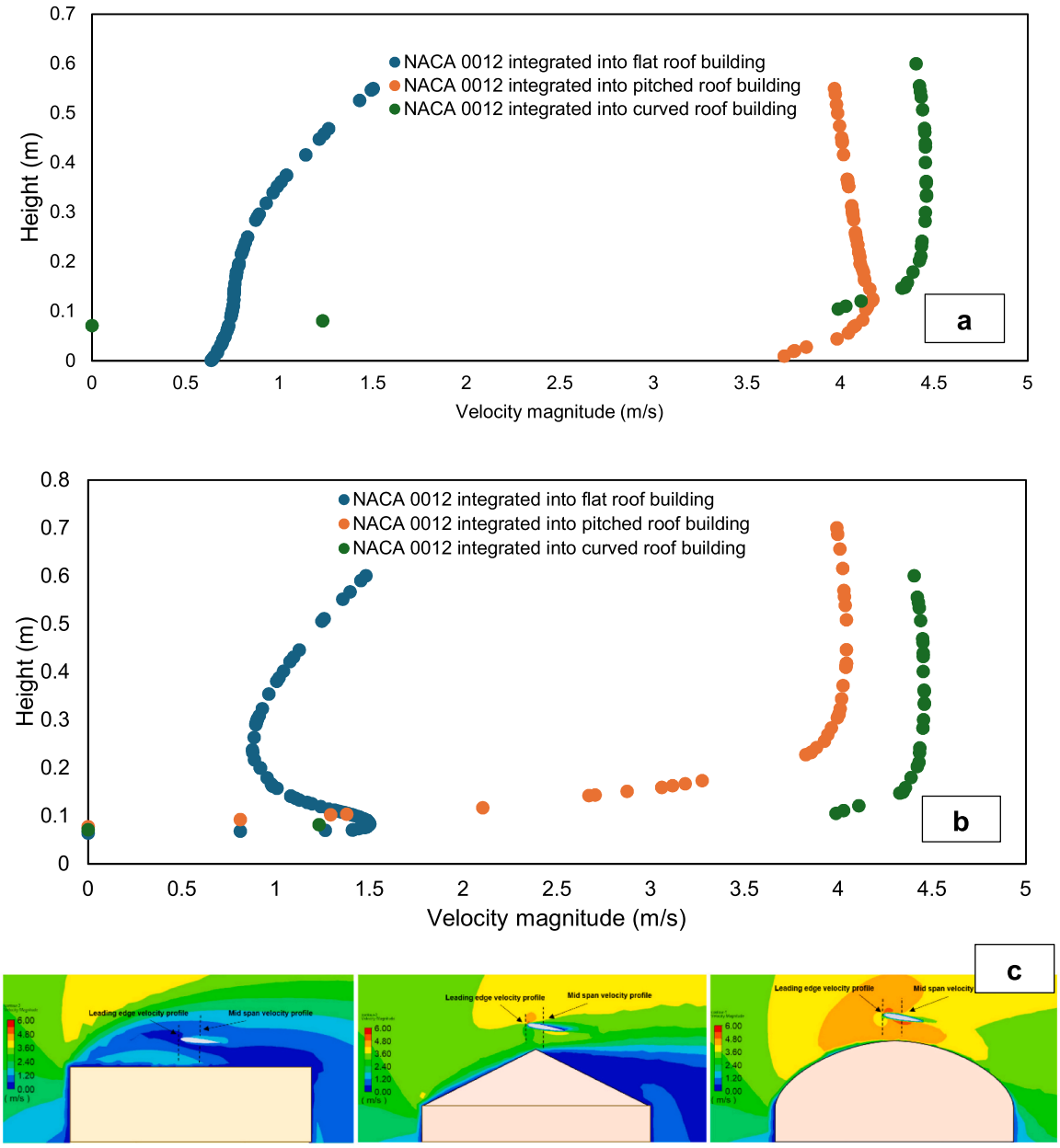

Fig. 13. Velocity profile located at the (a) leading edge (b) Mid span of the aerofoil (c) velocity profile points location for the three design parameters.

the curved roof building achieved the highest pitch angle of 6 degrees at 6 seconds, while the pitched roof integration attained approximately 4 degrees. Conversely, the flat roof integration exhibited the lowest pitch angle of 0.3 degrees. In conditions of higher wind speeds, such as 9 m/s, lower pitch angles are observed due to a reduced spring constant of constant 450 (n-m/rad) and increased oscillation frequency over time compared to lower wind speed scenarios, as shown in in (Fig. 14 c). Despite this, the NACA 0012 integrated into the curved roof building still achieved the highest pitch angle, reaching 4 degrees, followed by the pitched roof integration at 3.5 degrees. As anticipated, the flat roof integration yielded the lowest pitch angle, influenced by the roof shape and placement of the aerofoil within the flat roof structure.

The influence of wind speed and building roof shape on the dynamic behaviour of torque, angular velocity, and power output performance will be examined through a comparative analysis. Three different wind velocities including 3 m/s, 6 m/s, and 9 m/s will be investigated for three different models including the NACA 0012 aerofoil that is integrated into the flat, pitched, and curved roof building. Spring constant value of 850 (n-m/rad) was applied to the 1 degree-of-freedom (DOF) solver. The mechanical power output is determined by rotational movement, derived from the values of torque (**τ**) and angular velocity (**ω**), as depicted in Eq. (4).

$$P(t) = \tau.\omega \tag{4}$$

4.2.1.2. Torque. Fig. 15 (a) demonstrates the torque behaviour between an oscillating aerofoil with the NACA 0012 profile integrated into a flat, pitched, and curved roof under 3 m/s. From the results, it can clearly be observed that roof shapes can affect the torque behaviour under the same wind speed. The aerofoil incorporated into the curved roof building achieved the highest torque values, while the least values were seen from NACA 0012 installed into the flat roof building. While in Fig. 15 (b), the three different parameters were also simulated but under a higher wind speed, which was at 6 m/s. The findings suggest that installing the oscillating aerofoil with the NACA 0012 profile integrated into pitched and curved roof buildings also increases torque values

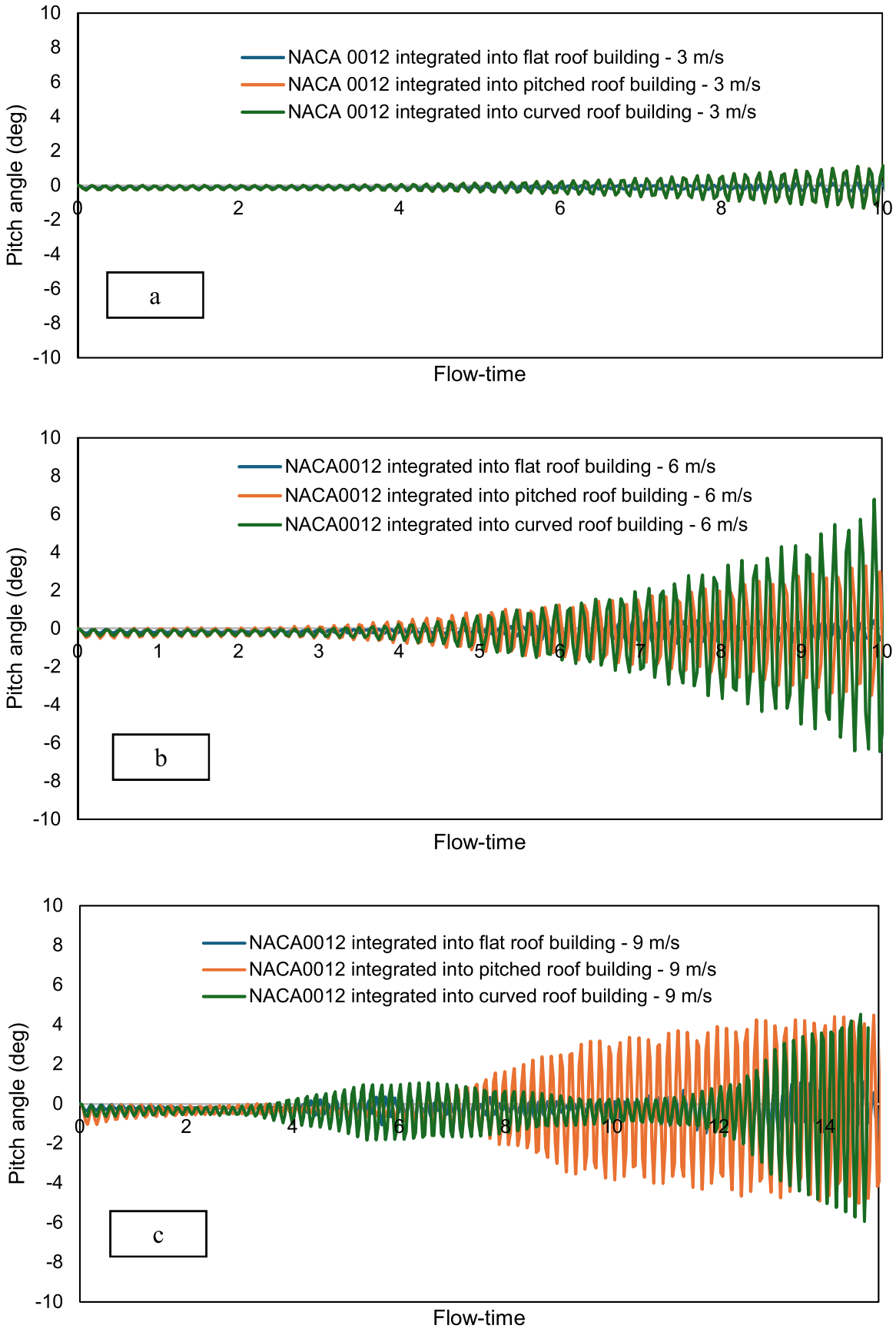

Fig. 14. Different pitch angle for an oscillating aerofoil with the NACA 0012 profile integrated into flat, pitched, and curved roof building under 3 m/s, 6 m/s, and 9 m/s.

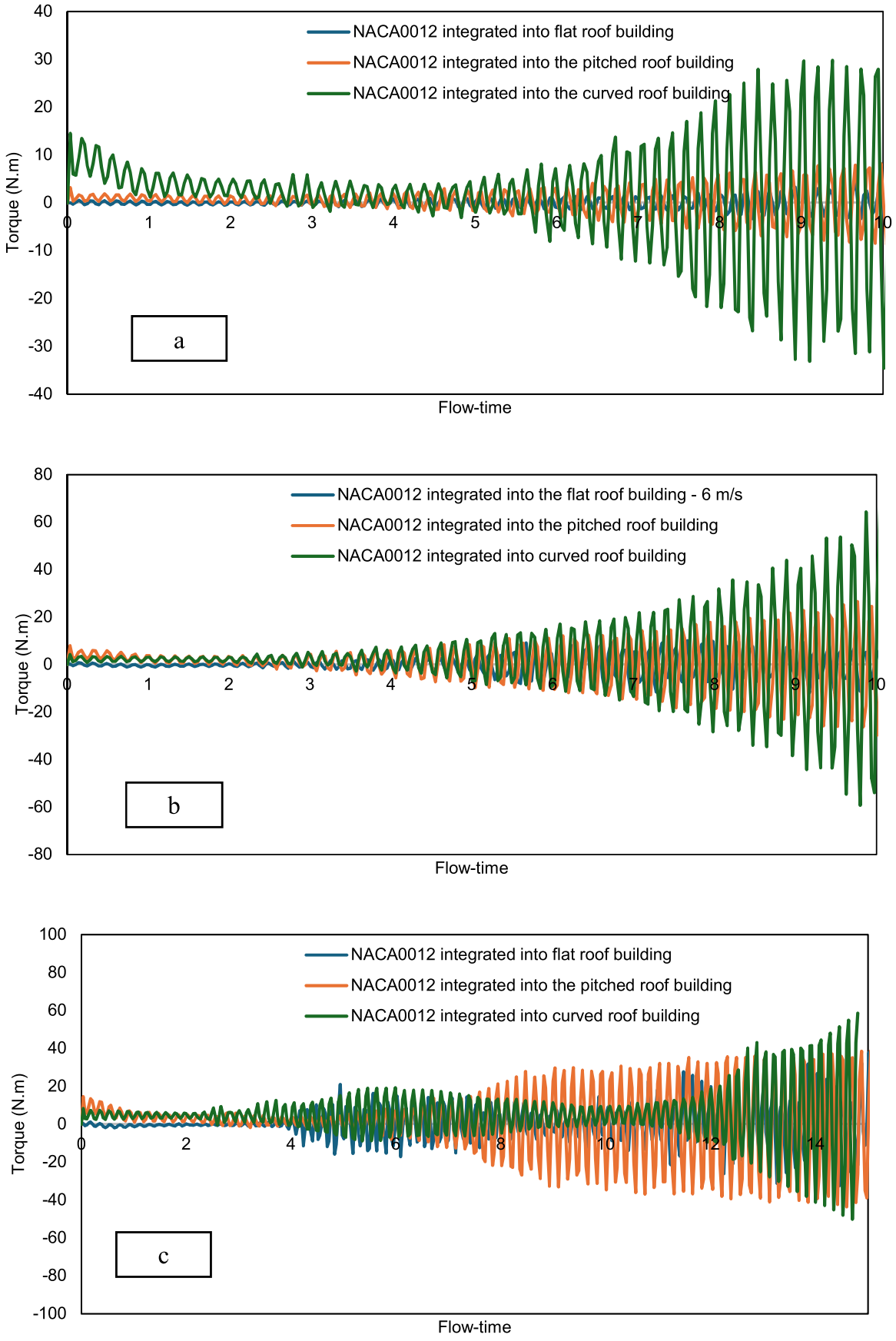

Fig. 15. Comparison of the torque between an oscillating aerofoil integrated into flat, pitched, and curved roof under (a) 3, (b) 6, and (c) 9 m/s.

under the same conditions and settings. The integration of an oscillating NACA 0012 on a curved and pitched roof structure demonstrated improved performance compared to a flat roof structure. These results indicate that the roof shape affects the performance of the oscillating aerofoil.

At an elevated wind speed of 9 m/s, illustrated in Fig. 15 (c), distinct behaviours emerge compared to lower wind speed scenarios at 3 m/s and 6 m/s. This deviation is primarily attributed to the reduction of the spring constant from 850 (n-m/rad) to 450 (n-m/rad), a strategic engineering decision aimed at maintaining stability at higher wind speeds, thereby ensuring the system overall performance and safety. Additionally, at 9 m/s wind speeds, the oscillating NACA 0012 aerofoil exhibits increased displacement, leading to significant disturbances in the wind flow, particularly noticeable when integrated into the curved roof building. In contrast, when integrated into a pitched roof building, windward side flow is prominent, albeit accompanied by flow separation. Hence, meticulous examination of the distance between the aerofoil and the curved roof is imperative to enhance the wind energy harvesting system efficiency. As depicted in Fig. 15 (c), the NACA 0012 integrated into the curved roof building initiates oscillations from time zero, with torque oscillations increasing after four flowtimes, gradually diminishing by the seventh flowtime, and subsequently surging again by the eleventh flowtime. This phenomenon is attributed to the roof shape, reduced spring constant value, increased displacement, and aerofoil placement above the building roof.

4.2.1.3. Angular velocity. The angular velocity graph shows that the curved roof NACA 0012 achieved the highest value under different wind speed such as 3, 6, and 9 m/s. The reason for this was the roof shape, the curved roof is known to have a higher acceleration rate of velocity magnitude as compared to the flat and pitched roof building. The angular velocity (ω) was calculated at the rate of angular displacement divided by the change in time, as shown in Eq. (5). Fig. 16 (a-c) demonstrates the comparison of angular velocity between different parameters including NACA 0012 installed into flat, pitched, and curved roof building structures under three different wind speeds.

$$\omega = \frac{\Delta\theta}{\Delta t} \tag{5}$$

Whereas in Fig. 16 (a-c), the angular velocity values for the simulated samples of flat, pitched, and curved roof building structures are presented under wind velocities of 3, 6 and 9 m/s. A comparison of the values demonstrates a considerable variation between the flat and curved roof structures incorporated with an oscillating aerofoil. This difference arises from the fluctuations in the pitch oscillation pattern over time. The pitch oscillations observed for the aerofoil integrated into a flat roof structure were comparatively lower than those experienced on a curved roof structure incorporating an oscillating NACA 0012 aerofoil. This difference is attributed to the flat roof building not encountering the same level of increased wind speed as the curved roof structure.

4.2.1.4. Potential power output. In ANSYS Fluent, torque computation is facilitated through momentum conservation equations derived from the Navier-Stokes equations. These equations capture the rotational force exerted on components such as blades or aerofoils, integrating pressure and viscous stress on their surfaces to provide insights into rotational dynamics and associated mechanical effects. Furthermore, in ANSYS CFD Fluent, power is determined utilizing the mechanical power equation, which involves the product of torque and angular velocity. These crucial values are directly extracted from the Fluent simulation results. Torque characterizes the rotational force acting on the system, while angular velocity denotes the rate of rotation. By multiplying these two parameters, the mechanical power exerted by the system is accurately computed. This meticulous approach ensures precise power calculations derived from the fluid dynamics simulations performed in ANSYS Fluent.

Fig. 17 (a) illustrates the average power output for three different parameters including oscillating NACA 0012 aerofoil integrated into flat, pitched, and curved roof structures at 3, 6, and 9 m/s. While in Fig. 17 (b), it demonstrates the average output for three different models in different wind directions. The stabilisation of power calculation in wind energy systems signifies the point where power output levels off, reaching a consistent and steady value with minimal fluctuation. This stabilisation coincides with a similar steadying of wind speed, indicating a consistent state of power generation. The recorded period, commencing from the initiation of the first oscillation and extending from 0.035 to 20 flow time, encapsulates wind speed variations and their impact on power generation within this timeframe. Analysing power output during this recorded period provides valuable insights into how wind speed fluctuations influence power generation and reveals the point at which power stabilises within the specified flow time. Understanding this stabilisation concerning wind speed fluctuations is pivotal for evaluating wind energy harvesting system performance, ensuring safe and efficient operation, and optimising energy production within wind energy systems.

The findings indicate that the integration of an oscillating NACA 0012 aerofoil into a curved roof configuration yielded the highest average power output across various wind speeds. Fig. 17 (a) illustrates this outcome, with the curved roof structure coupled with the oscillating aerofoil achieving an average power output of 18 W. Conversely, the lowest power output values were observed for the oscillating NACA 0012 aerofoil integrated into a flat roof, registering only 0.6 W at 3 m/s wind speed.

Moreover, the mechanical power output reached its peak at 18 W when the NACA 0012 aerofoil was integrated into the curved roof building, highlighting the significant impact of roof shape on power efficiency. In addition, the NACA 0012 integrated into the pitched roof configuration at 9 m/s wind speed achieved (12 W) under 9 m/s. The results also highlight the influence of wind speed on the performance of wind energy harvesting systems. As wind speed increases from 3 m/s to 9 m/s, an improvement in power output is observed for the NACA 0012 integrated into flat roof buildings. This emphasizes the crucial role of wind speed in determining the efficiency of energy harvesting systems, with higher wind speeds correlating to higher average mechanical power output.

Furthermore, the study highlights the substantial impact of altering roof shape and aerofoil placement on the power efficiency of building roof structures. Specifically, the curved roof configuration demonstrates superior power extraction performance compared to flat and pitched roof scenarios. This underscores the importance of considering aerodynamic design elements in optimizing energy harvesting systems. Also, the sensitivity analysis conducted emphasizes the significance of factors such as roof shape, wind velocity, and system placement in influencing energy harvesting performance. It suggests the need for further investigation into the sensitivity analysis of parameters such as spring constant in various conditions to identify optimal values for enhanced performance.

In conclusion, the study illustrates the critical role of roof shape, aerofoil placement, and wind speed in determining the efficiency of wind energy harvesting systems. The findings provide valuable insights for optimizing energy extraction and highlight avenues for future research to enhance system performance.

4.2.2. Impact of wind directions

As shown in Fig. 17 (b), an examination was conducted to assess how various wind directions affect the power output of an oscillating aerofoil with the NACA 0012 profile integrated into building roof. A sensitivity analysis was performed on the power output, considering three parameters: the NACA 0012 profile, installed in three distinct roof shapes including flat, pitched, and curved. Simulations were conducted for four different wind directions (0 degrees, 10 degrees, 15 degrees, and 25 degrees) at 3 m/s. The study aimed to explore the effect of changes in

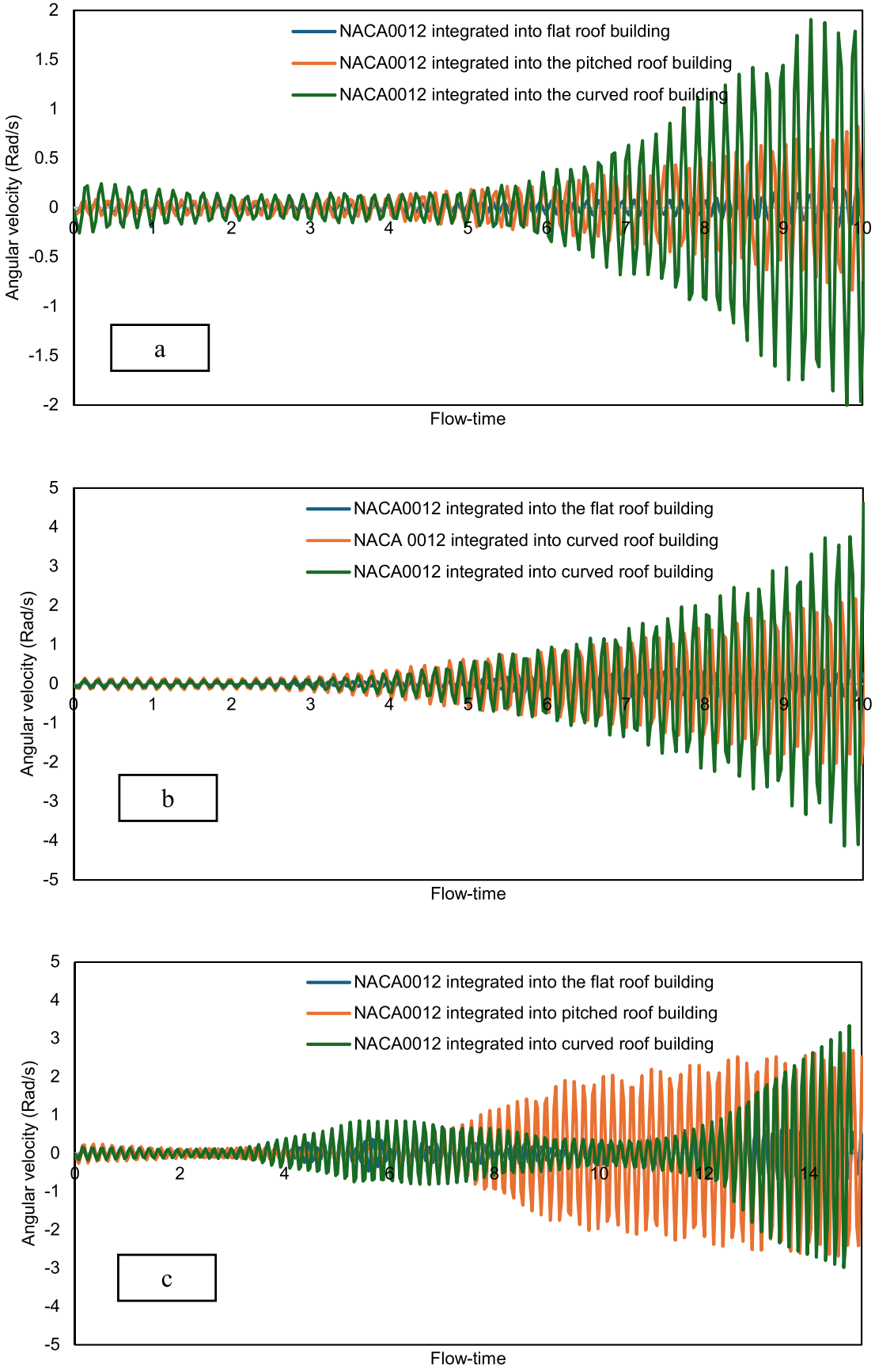

Fig. 16. Comparison of the angular velocity between an oscillating aerofoil integrated into flat, pitched, and curved roof under (a) 3, (b) 6, and (c) 9 m/s.

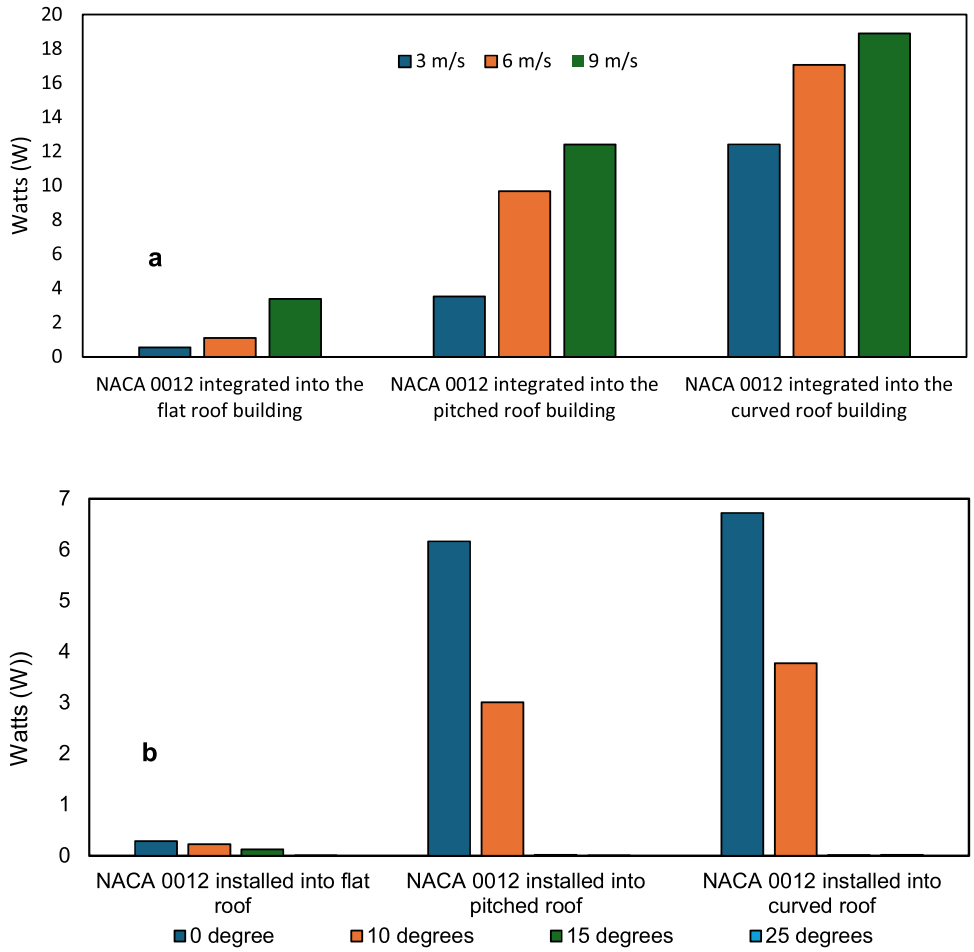

Fig. 17. Average power output for three different models under different (a) wind speeds and (b) wind directions.

wind direction on the power output efficiency of the NACA 0012 aerofoil in diverse roof structures, including flat, pitched, and curved designs. The findings offer valuable insights into the aerodynamic behaviour and potential for power generation. Notably, critical observations highlight the impact of wind direction in determining power output. Specifically, a decline in power output was observed starting at 10 degrees and persisting up to 25 degrees of wind direction, highlighting the significance of the angle of wind incidence on power generation.

This comprehension is crucial for optimising the placement and orientation of an oscillating aerofoil wind energy harvesting system on various roof structures, ultimately enhancing overall power efficiency. The results obtained from various roof structures, specifically the contrasting performance between flat, pitched, and curved roofs, highlight the critical role of a building architecture in wind energy generation. Flat roofs exhibit inefficiencies due to wind recirculation and shear effects, emphasising the need for strategic placement to mitigate these drawbacks. In contrast, pitched and curved roofs demonstrate improved power output, capitalising on wind speed acceleration facilitated by their design. This highlights the potential for enhancing wind energy utilisation by aligning the oscillating aerofoil wind energy harvesting design and placement with the building structure. Furthermore, the positioning and angle of attack of integrated aerofoils relative to wind direction significantly influence system performance. In summary, wind direction's impact on oscillating wind energy systems requires consideration during design and operation to optimise energy harvesting capabilities.

4.2.3. Power spectral density vs frequency

The Power Spectral Density (PSD) vs frequency plot offers valuable insights into the behaviour of an oscillating aerofoil integrated into a building roof structure under varying wind speeds. This plot illustrates how the distribution of power across different frequencies reflects changes in aerodynamic forces acting on the aerofoil. Understanding the PSD plot provides crucial information about the dynamics of the aerofoil response to wind, aiding in the design and optimization of structures for improved performance and safety. In summary, the PSD vs frequency plot provides insights into how the aerodynamic forces acting on the oscillating aerofoil integrated into the building roof structure vary with wind speed, showing the frequency content and intensity of these forces at different wind speeds.

Fig. 18 (a-c) show the PSD vs frequency in three different wind speeds including 3 m/s, 6 m/s, and 9 m/s for the three design parameters of an oscillating aerofoil integrated into the flat, pitched, and curved roof building. The Fig. 18 (b and c) presents a low value of PSD against frequency, and its peak can be observed at 5.8 Hz in 9 m/s for both NACA 0012 integrated into the pitched and curved roof building. While in Fig. 18 (a), a very unstable PSD behaviour can be observed from 0 Hz to 8 Hz for NACA 0012 integrated into the flat roof building. In this case (flat), a constant 850 (n-m/rad) for 3 m/s wind speed and 450 (n-m/rad) for 9 m/s wind speed, it indicates that the system has higher damping at 3 m/s. This higher damping would suppress oscillations more effectively, resulting in a lower amplitude of response overall. Therefore, despite the higher wind speed at 9 m/s, the lower damping allows for more significant oscillations and potentially higher peaks in the PSD vs frequency plot compared to the 3 m/s wind speed, where higher damping suppresses oscillations and reduces the peak in the PSD plot.

Reducing the spring constant from constant 850 (n-m/rad) to 450 (n-m/rad) to maintain stability at higher wind speeds is a reasonable

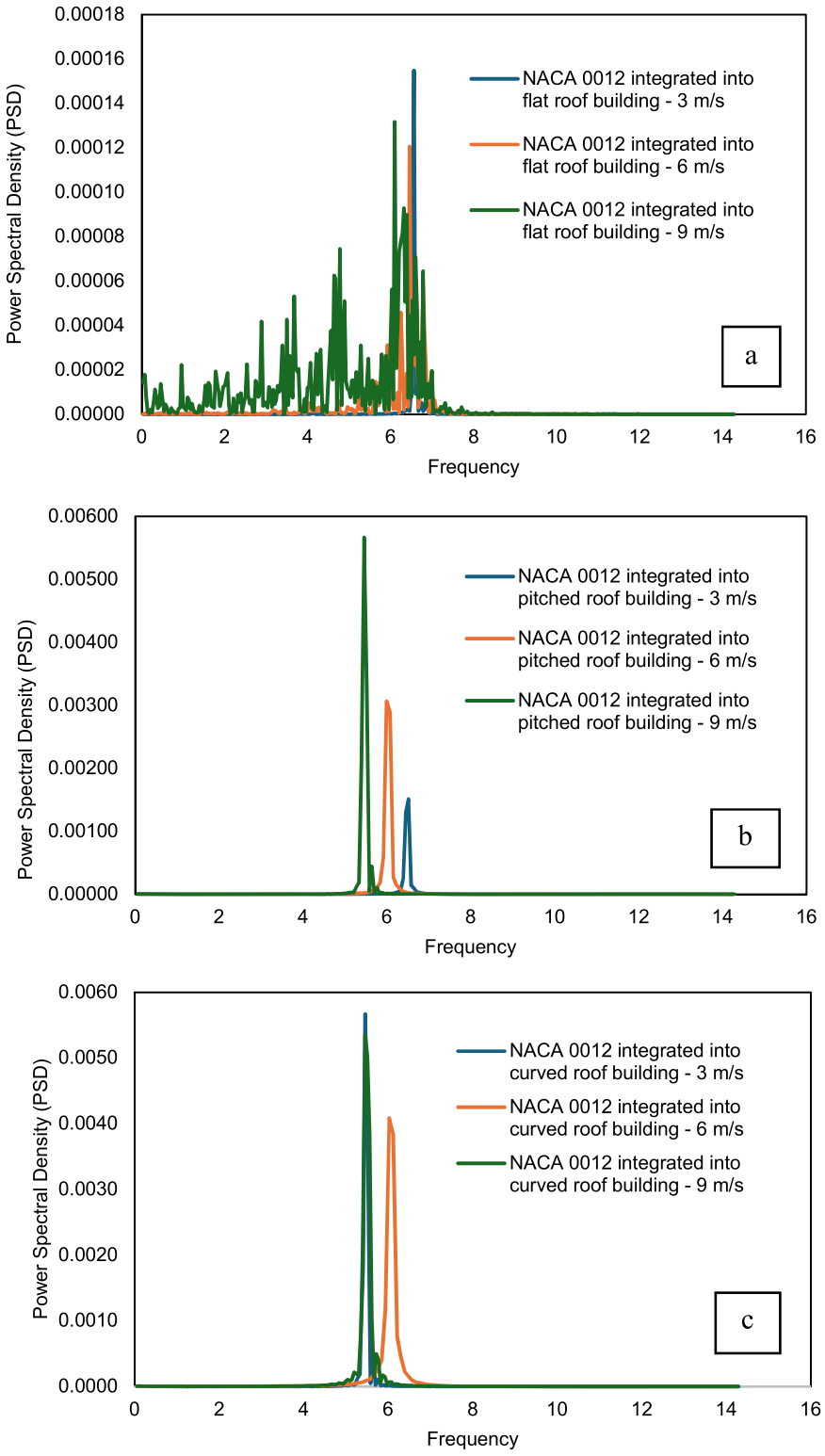

Fig. 18. Power Spectral Density vs Frequency NACA 0012 integrated into (a) flat, (b) pitched, and (c) curved roof building under 3 m/s, 6 m/s, and 9 m/s.

engineering decision aimed at ensuring the overall performance and safety of the system. Through decreasing the stiffness of the system, engineers can enhance its ability to absorb energy from wind-induced vibrations and mitigate the risk of instability or excessive oscillations. This adjustment allows for greater flexibility and damping, which can improve the dynamic response of the system and prevent it from reaching critical levels of instability as wind speeds increase. While this approach addresses the immediate concern of stability at higher wind speeds, engineers must carefully consider potential trade-offs in the system's response to lower wind speeds and its overall structural integrity. Through modelling and simulation studies, engineers can analyze the behaviour of the system under various conditions and optimize design parameters to achieve an optimal balance between stability, dynamic response, and structural integrity.

The Power Spectral Density (PSD) value of 0.0059 achieved at 9 m/s for the oscillating aerofoil NACA 0012 integrated into the curved roof

building indicates the intensity of the aerodynamic forces experienced by the aerofoil. This higher PSD value suggests that at this wind speed, the aerofoil is subjected to significant fluctuations in aerodynamic forces, which is due to the interaction between the aerofoil shape and the curved roof structure. On the other hand, achieving a nearly identical PSD value of 0.0058 for the oscillating aerofoil NACA 0012 integrated into the pitched roof building suggests that, despite differences in the building, the aerodynamic forces experienced by the aerofoil are comparable between the two configurations. This implies that factors other than the roof shape, such as the angle of attack, wind flow patterns, or turbulence, may play significant roles in determining the aerodynamic response of the aerofoil. Further analysis would be needed to explain the specific mechanisms behind these observations and their implications for the design and performance of the integrated aerofoil systems.

While the lowest value was achieved by the PSD value of less than 0.00002 achieved at 6 m/s for the oscillating aerofoil NACA 0012 integrated into the flat roof building, this indicates relatively lower intensity of aerodynamic forces compared to the other roof configurations, as shown in Fig. 18 (a). The disparity in PSD values among the three roof types suggests varying degrees of aerodynamic interaction between the aerofoil and the different roof structures. The higher PSD values for the curved and pitched roof buildings suggest potentially more complex airflow patterns and greater aerodynamic loading on the aerofoil compared to the flat roof configuration. However, the nearly identical PSD values of 0.0059 and 0.0058 for the curved and pitched roof buildings at the same wind speed indicate similar aerodynamic responses despite their structural differences, as shown in Fig. 18 (b-c). This implies that factors beyond roof shape, such as angle of attack, wind flow patterns, or turbulence, may significantly influence the aerodynamic behaviour of the integrated aerofoil systems. Further investigation into these factors is essential for optimizing the design and performance of such integrated systems in various architectural contexts.

5. Conclusion and future works

This study introduced a model for a Building Integrated Wind Energy Harvesting System (BI-WEHS) and investigated the dynamics of power capture and fluid-structure interactions. Through rigorous investigation, key results and findings were identified, specific gaps in knowledge were identified, and significant outcomes were highlighted. These include:

- The absence of comprehensive studies on wind energy harvesting systems integrated into building roof structures, hindering direct comparisons. Existing research primarily focuses on building integrated wind turbines rather than specific roof integration.
- The research methodology employed in existing studies lacks a dynamic mesh with one degree of freedom, with most studies concentrating on assessing the impact of placement and wind speed acceleration facilitated by the building roof shape.
- The study created a Computational Fluid Dynamics (CFD) model for the oscillating aerofoil wind energy harvesting system. A one-degree-of-freedom (1 DOF) solver was utilized to evaluate dynamic characteristics and power extraction efficiency.
- The use of ANSYS Fluent and a 1 DOF solver enabled the prediction of values for average mechanical power output, torque, and angular velocity.
- Numerical analysis reveals that integrating an oscillating NACA 0012 aerofoil into a curved roof yields the highest average power output. Specifically, the curved roof integrated with the aerofoil achieves 18 W at 9 m/s, while the flat roof records the lowest average power outout of 0.6 W at 3 m/s wind speed. Integration of the oscillating aerofoil into a pitched roof achieves 12 W at 9 m/s.
- Critical observations highlight the impact of wind direction in determining power output. Specifically, a decline in power output was observed starting at 10 degrees and persisting up to 25 degrees of wind direction, highlighting the significance of the angle of wind incidence on power generation.
- This study contributes to a thorough understanding of the interaction between airflow and an integrated model of an oscillating rigid aerofoil and building roof in diverse parameters and boundary conditions.

The research described in this manuscript also establishes the groundwork for future studies, outlining specific areas for further exploration as follows:

- Investigate the alternative shapes of the aerofoil, such as non-symmetrical or low Reynolds number aerofoil profile sections, when integrated into different roof building structures.
- Examine the influence of various dimensions of the aerofoil chord length and span on power and energy capture efficiency.
- Conduct research on power performance under two degrees of freedom motion, including pitch and heave.
- Examine the influence of various turbulence intensities on the operation and life expectancy of the technology.

- Future endeavours should concentrate on overcoming existing limitations by establishing standardized experimental protocols and methodologies for the study of building-integrated wind energy systems. This approach will enhance comparability across studies and deepen our understanding of the factors impacting system performance.
- Sensitivity analyses across damping spring constant values and exploration of adjacent structures' effects on system efficiency are areas for future investigation.
- Understand turbulence intensity and vortices generated during the interaction between the aerofoil and its surroundings is crucial for comprehending motion influences.
- Explore different case studies across various environments will provide valuable insights into system performance and applicability.

CRediT authorship contribution statement

Katrina Calautit: Writing – original draft, Methodology, Conceptualization. **Cameron Johnstone:** Writing – review & editing, Supervision.

Declaration of Competing Interest

The authors declare that there are no conflicts of interest or personal affiliations that could have influenced the research presented in this paper.

Data Availability

Data will be made available on request.

Acknowledgement

The Ph.D. research program acknowledges with gratitude the funding support from the Mechanical and Aerospace Engineering Department at the University of Strathclyde.

Appendix A. Supporting information

Supplementary data associated with this article can be found in the online version at doi:10.1016/j.egyr.2024.04.022.

References

Abdelkefi, A., Hajj, M.R., Nayfeh, A.H., 2012. Sensitivity analysis of piezoaeroelastic energy harvesters. J. Intell. Mater. Syst. Struct. 23 (13), 1523–1531.

Abdessemed, C., Yao, Y., Abdessalem, B., Narayan, P., 2018. Morphing airfoils analysis using dynamic meshing. Int. J. Numer. Methods Heat. Fluid Flow. (5).

Abdizadeh, G., Farokhinejad, M., Ghasemloo, S., 2022. Numerical investigation on the aerodynamic efficiency of bio-inspired corrugated and cambered airfoils in ground effect. Sci. Rep. 12, 19117.

I. Abohela, N. Hamza, S. Dudek. Roof Mounted Wind Turbines: The influence of roof shape, building height and urban location on wind speed, *Passive and Low Energy Architecture - 28th Conference, Perú* 2012.

Akaydin, H.D., Elvin, N., Andreopoulos, Y., 2012. The performance of a self-excited fluidic energy harvester. Smart Mater. Struct. 21 (2), 025007.

Alrawashdeh, H., Stathopoulos, T., 2020. Wind loads on solar panels mounted on flat roofs: effect of geometric scale. J. Wind Eng. Ind. Aerodyn. 206, 104339.

ANSYS 12.0, Six DOF (6DOF) Solver Theory, 2009 (Accessed at: ⟨https://www.afs.enea.it/project/neptunius/docs/fluent/html/th/node41.htm⟩ [Accessed: 10-Jan-2023].

Aquino, A., Calautit, J.K., Hughes, B., 2017a. Urban integration of aeroelastic belt for low-energy wind harvesting. Energy Procedia 105, 738–743.

Aquino, A.I., Calautit, J.K., Hughes, B.R., 2017a. Evaluation of the integration of the Wind-Induced Flutter Energy Harvester (WIFEH) into the built environment: experimental and numerical analysis. Appl. Energy 207, 61–77.

Aquino, A.I., Calautit, J.K., Hughes, B.R., 2017b. Integration of aero-elastic belt into the built environment for low-energy wind harnessing: Current status and a case study. Energy Convers. Manag. 149, 830–850.

Aravindhan, N., Natarajan, M.P., Ponnuvel, S., Devan, P.K., 2022. Recent developments and issues of small-scale wind turbines in urban residential buildings - a review. Energy Environ. 34 (4), 1142–1169.

Ayhan, D., Sağlam, S., 2012. A technical review of building-mounted wind power systems and a sample simulation model. Renew. Sustain. Energy Rev. 16 (1), 1040–1049.

Batay, S., Baidullayeva, A., Zhao, Y., Wei, D., Baigarina, A., Sarsenov, E., Shabdan, Y., 2024. Aerostructural design optimization of wind turbine blades. Processes 12, 22.

Bhat, S., Govardhan, R., 2013. Stall flutter of NACA 0012 airfoil at low Reynolds numbers. J. Fluids Struct. 41, 166–174.

A. Bibo. Investigation of Concurrent Energy Harvesting from Ambient Vibrations and Wind, PhD Thesis, Clemson University, 2014.

Bryant, M., Mahtani, R.L., Garcia, E., 2012b. Wake synergies enhance performance in aeroelastic vibration energy harvesting. J. Intell. Mater. Syst. Struct. Vol. 23 (No. 10), 1131–1141.

Bryant, M., Shafer, M., Garcia, E., 2012a. Power and efficiency analysis of a flapping wing wind energy harvester. Proc., Act. Passiv. Smart Struct. Integr. Syst. 8341.

Calautit, K., Aquino, A., Calautit, J.K., Nejat, P., Jomehzadeh, F., Hughes, B.R., 2018. A review of numerical modelling of multi-scale wind turbines and their environment. Computation 6 (1), 24.

Calautit, J.K., Hughes, B.R., 2014. Wind tunnel and CFD study of the natural ventilation performance of a commercial multi-directional wind tower. Build. Environ. 80, 71–83.

Calautit, K., Johnstone, C., 2023. State-of-the-art review of micro to small-scale wind energy harvesting technologies for building integration. Energy Convers. Manag.: X 20, 100457.

Cao, Y., Taslimi, M., Dastjerdi, S.M., Ahmadi, P., Ashjaee, M., 2022. Design, dynamic simulation, and optimal size selection of a hybrid solar/wind and battery-based system for off-grid energy supply. Renew. Energy 187, 1082–1099.

Cao, W., Wang, X., Liu, Y., Yin, Y., Yang, J., An, J., 2023. Large eddy simulation on wind-induced interference effects of staggered chamfered square cylinders. Sci. Rep. 13 (1), 17532.

Chai, Y., Gao, W., Ankay, B., Li, F., Zhang, C., 2021b. Aeroelastic analysis and flutter control of wings and panels: a review. Int. J. Mech. Syst. Dyn. 1, 5–34.

Chai, Y., Gao, W., Ankay, B., Li, F., Zhang, C., 2021a. Aeroelastic analysis and flutter control of wings and panels: a review. Int. J. Mech. Syst. Dyn. 1 (2), 5–34.

Cheng, P., Huang, Y., Wan, D., 2019. A numerical model for fully coupled aero-hydrodynamic analysis of floating offshore wind turbine. Ocean Eng. 173, 183–196.

Chong, W.T., Pan, K.C., Poh, S.C., Fazlizan, A., Oon, C.S., Badarudin, A., Nik-Ghazali, N., 2013. Performance investigation of a power augmented vertical axis wind turbine for urban high-rise application. Renew. Energy 51, 388–397.

Dunbar, A., Craven, B., Paterson, E., 2015. Development and validation of a tightly coupled CFD/6-DOF solver for simulating floating offshore wind turbine platforms. Ocean Eng. 110, 98–105.

Fangwei, H., Sarkar, P., 2018. A time-domain method for predicting wind-induced buffeting response of tall buildings. J. Wind Eng. Ind. Aerodyn. 182, 61–71.

Fu, C., Uddin, M., Zhang, C., 2020. Computational Analyses of the Effects of Wind Tunnel Ground Simulation and Blockage Ratio on the Aerodynamic Prediction of Flow over a Passenger Vehicle. Vehicles 2, 318–341.

Gao, Y., Xie, L., Lam, T.L., 2022. A novel and more efficient oscillating foil for wave-driven unmanned surface vehicles. Front. Robot. AI 15 (9), 759200.

Hamlehdar, M., Kasaeian, A., Safaei, M.R., 2019. Energy harvesting from fluid flow using piezoelectrics: A critical review. Renew. Energy 143, 1826–1838.

Hernandez-Estrada, E., Lastres-Danguillecourt, O., Robles-Ocampo, J., Lopez-Lopez, A., Sevilla-Camacho, P., Perez-Sariñana, B., Dorrego-Portela, J., 2021. Considerations for the structural analysis and design of wind turbine towers: a review. Renew. Sustain. Energy Rev. 137, 110447.

J.D. Hobeck. Energy Harvesting with Piezoelectric Grass for Autonomous Self-Sustaining Sensor Networks, Thesis, A dissertation submitted in partial fulfilment of the requirements for the degree of Doctor of Philosophy (Aerospace Engineering) in The University of Michigan 2014.

Jamil, M., Javed, A., Shah, S.I.A., Mansoor, M., Hameed, A., Djidjeli, K., 2020. Performance analysis of flapping foil flow energy harvester mounted on piezoelectric transducer using meshfree particle method. J. Appl. Fluid Mech. 13 (6), 1859–1872.

Jaohindy, P., McTavish, S., Garde, F., Bastide, A., 2013. An analysis of the transient forces acting on Savonius rotors with different aspect ratios. Renew. Energy 55, 286–295.

Kim, J., Magee, A., Guan, K., Y, H., CFD Simulation of Flow-Induced Motions of a Multi-Column Floating Platform. *Proceedings of the ASME 2011 30th International Conference on Ocean*, Offshore and Arctic Engineering. Volume 7: CFD and VIV; Offshore Geotechnics. Rotterdam, The Netherlands, pp. 319-326, 2011.

Ledo, L., Kosasih, P.B., Cooper, P., 2011. Roof mounting site analysis for micro-wind turbines. Renew. Energy 36 (5), 1379–1391.

Li, K., Yang, Z., Gu, Y., He, S., Zhou, S., 2018. Nonlinear magnetic-coupled flutter-based aeroelastic energy harvester, Modeling, simulation and experimental verification. Smart Mater. Struct. 28 (1), 015020.

Lu, L., Ip, K.Y., 2009. Investigation on the feasibility and enhancement methods of wind power utilization in high-rise buildings of Hong Kong. Renew. Sustain. Energy Rev. 13 (2), 450–461.

Maalouly, M., Souaiby, M., ElCheikh, A., Issa, J.S., Elkhoury, M., 2022. Transient analysis of H-type vertical axis wind turbines using CFD. Energy Rep. 8, 4570–4588.

McCarthy, J.M., Watkins, S., Deivasigamani, A., John, S.J., 2016. Fluttering energy harvesters in the wind: a review. J. Sound Vib. 361, 355–377.

Menon, K., Mittal, R., 2019. Flow physics and dynamics of flow-induced 1 pitch oscillations of an airfoil. J. Fluid Mech. 877, 582–613.

Naseer, R., Dai, H., Abdelkefi, A., Wang, L., 2017. Piezomagnetoelastic energy harvesting from vortex-induced vibrations using monostable characteristics. Appl. Energy 203, 142–153.

Ntinas, G.K., Zhang, G., Fragos, V.P., Bochtis, D.D., Nikita-Martzopoulou, C., 2014. Airflow patterns around obstacles with arched and pitched roofs: Wind tunnel measurements and direct simulation. JEur. J. . Mech. - B/Fluids 43, 216–229.

Østergaard, P.A., Duic, N., Noorollahi, Y., Kalogirou, A., 2021. Recent advances in renewable energy technology for the energy transition. Renew. Energy 179, 877–884.

Patel, M., Henderson, A., 2003. On the modeling of a floating offshore wind turbine. Wind Energy 6, 53–76.

Poirel, D., Harris, Y., Benaissa, A., 2008. Self-sustained aeroelastic oscillations of a NACA0012 airfoil at low-to-moderate Reynolds numbers. J. Fluids Struct. 24 (5), 700–719.

Quy, V.D., Sy, N.V., Hung, D.T., Huy, V.Q., 2016. Wind tunnel and initial field tests of a micro generator powered by fluid-induced flutter. Energy Sustain. Dev. 33, 75–83.

Rad, M.P., Khoshnevis, A.B., 2023. Experimental investigation of flow structure over pitching airfoil in the wake of circular cylinder. Ocean Eng. 284, 115103.

Reja, R.K., Amin, R., Tasneem, Z., Ali, M.F., Islam, M.R., Saha, D.K., Badal, F.R., Ahamed, M.H., Moyeen, S.I., Das, S.K., 2022. A review of the evaluation of urban wind resources: challenges and perspectives. Energy Build. 257 (2), 111781.

S. Roothaan, C. Williams, S. Guerrero, P. Acioli. Optimization of Small Scale Wind Turbine in Urban Areas, *Conference: Society for Advancement of Hispanics/Chicanos and Native Americans in Science National Conference*, (2012).

N. Rostamzadeh, R. Kelso, B. Dally, Z. Tian. An Experimental and Computational Study of Flow over a NACA 0021 Airfoil with Wavy Leading Edge Modification, *Conference: 18th Australasian Fluid Mechanics Conference At: Launceston*, (2012).

Sanderasagran, A., Azizuddin, A., Oumer, A., 2020. Comparative CFD power extraction analysis of novel nature inspired vertical axis wind turbines Comparative CFD power extraction analysis of novel nature inspired vertical axis wind turbines. IOP Conf. Ser. Mater. Sci. Eng. 863 (1).

Sazesh, S., Shams, S., 2017. Nonlinear aeroelastic analysis of an airfoil with control surface free-play using stochastic approach. J. Fluids Struct. 72, 114–126.

Shuang, L., Zhang, L., Xu, J., Yang, K., J, Juanjuan, S., Guangxing, G., 2020. Experimental investigation of a pitch-oscillating wind turbine airfoil with vortex generators. J. Renew. Sustain. Energy 12 (6), 063304.

Steenwijk, B., Druetta, P., 2023. Numerical Study of Turbulent Flows over a NACA 0012 Airfoil: Insights into Its Performance and the Addition of a Slotted Flap. Appl. Sci. 13 (13), 7890.

Tan, J.H.C., Magee, A., Kim, J.W., Teng, Y.J., Zukni, N.A., 2013. CFD Simulation for Vortex Induced Motions of a Multi-Column Floating Platform. Proc. ASME 2013 32nd Int. Conf. Ocean, Offshore Arct. Eng. 7.

Tang, D., Dowell, E.H., 2016. Experimental aeroelastic models design and wind tunnel testing for correlation with new theory. Aerospace 3 (2), 12.

Toja-Silva, F., Kono, T., Peralta, C., Lopez-Garcia, O., Chen, J., 2018. A review of computational fluid dynamics (CFD) simulations of the wind flow around buildings for urban wind energy exploitation. J. Wind Eng. Ind. Aerodyn. 180, 66–87.

Tran, T., Kim, D., Song, J., 2014. Computational Fluid Dynamic Analysis of a Floating Offshore Wind Turbine Experiencing Platform Pitching Motion. Energies 7 (8), 5011–5026.

Walker, S.L., 2011. Building mounted wind turbines and their suitability for the urban scale—a review of methods of estimating urban wind resource. Energy Build. 43 (8), 1852–1862.

Wang, Y., Chen, X., 2022. Extraction of aerodynamic damping and prediction of vortex-induced vibration of bridge deck using CFD simulation of forced vibration. J. Wind Eng. Ind. Aerodyn. 224, 104982.

Wang, B., Li, Y., Gao, S., Hu, S., Kanmin, Z., Zheng, X., 2022. Motion characteristics and aero-elastic responses of floating offshore wind turbine under coupling action of waves and winds. Front. Environ. Sci. 10.

Wang, Q., Wang, J., Hou, Y., Yuan, R., Luo, K., Fan, J., 2018. Micrositing of roof mounting wind turbine in urban environment: CFD simulations and lidar measurements. Renew. Energy 115, 1118–1133.
Wicaksono, H., Hadi, S., Pranoto, B., Fakhruddin, M., 2021. Initial rotation characteristic investigation of a hybrid savonius - darrieus wind turbine using 6 DOF computational fluid dynamics. Mek.: Maj. Ilm. Mek. 20 (1), 9–17.
Willis, D.J., Niezrecki, C., Kuchma, D., Hines, E., Arwade, S.R., Barthelmie, R.J., DiPaola, M., Drane, P.J., Hansen, C.J., Inalpolat, M., Mack, J.H., Myers, A.T., Rotea, M., 2018. Wind energy research: state-of-the-art and future research directions. Renew. Energy 125, 133–154.
Xu, S., Gao, Z., Xue, W., 2022. CFD database method for roll response of damaged ship during quasi-steady flooding in beam waves. Appl. Ocean Res. 126, 103282.
Xu, W., Li, Y., Li, G., Li, S., Zhang, C., Wang, F., 2021a. High-resolution numerical simulation of the performance of vertical axis wind turbines in urban area: part II, array of vertical axis wind turbines between buildings. Renew. Energy 176, 25–39.
Xu, W., Li, G., Zheng, X., Li, Y., Li, S., Zhang, C., Wang, F., 2021b. High-resolution numerical simulation of the performance of vertical axis wind turbines in urban area: Part I, wind turbines on the side of single building. Renew. Energy 177, 461–474.
Xu, Z., Yin, J., 2023. The Influence of Aeroelastic Effects on Wind Load and Wind-Induced Response of a Super-Tall Building: An Experimental Study. Buildings 13 (7), 1871.
Yu-Hsien, L., Ahmad, H., 2022. Transient analysis of the slamming wave load on an offshore wind turbine foundation generated by different types of breaking waves. J. Renew. Sustain. Energy 14, 053302.
Zhang, Y., Zhou, Z., Wang, K., Li, X., 2020. Aerodynamic characteristics of different airfoils under varied turbulence intensities at low reynolds numbers. SAppl. Sci. 10, 1706.
L. Zhao, Small-scale wind energy harvesting using piezoelectric materials, PhD thesis, Nanyang Technological University, Singapore, 2015.
Zhao, L., Yang, Y., 2015. Enhanced aeroelastic energy harvesting with a beam stiffener. Smart Mater. Struct. 24 (3), 032001.
Zhu, Q., Wang, X., Demartino, C., Cristoforo, Y., Yan, J., 2023b. Revealing aeroelastic effects on low-rise roof structures in turbulent winds via isogeometric fluid–structure interaction. Comput. Mech. 72, 1–16.
Zhu, Q., Wang, X., Demartino, C., Yan, J., 2023a. Revealing aeroelastic effects on low-rise roof structures in turbulent winds via isogeometric fluid–structure interaction. Comput. Mech. 72 (6), 1175–1190.
Zhu, H., Zhou, D., Han, Z., Ma, J., Bao, Y., Fu, S., 2020. The performance assessment of a semisubmersible platform subjected to wind and waves by a CFD/6-DOF approach. Flow-induced vibration control and energy harvesting. Shock Vib. 2020 (2), 1–16.